TÜBİTAK

Turkish Journal of Earth Sciences

http://journals.tubitak.gov.tr/earth/

Research Article

Turkish J Earth Sci
(2022) 31: 260-283

doi:10.3906/yer-2111-18

Hydrochemical characteristics and geothermometry applications of thermal waters in the Çürüksu Graben, western Turkey

Ali GÖKGÖZ[1,*], Halim MUTLU[2], Mehmet Ali AKMAN[1]

[1]Department of Geological Engineering, Engineering Faculty, Pamukkale University, Denizli, Turkey
[2]Department of Geological Engineering, Engineering Faculty, Ankara University, Ankara, Turkey

Received: 28.11.2021 • **Accepted/Published Online:** 28.03.2022 • **Final Version:** 18.05.2022

Abstract: In this study, we investigate chemical and isotopic characteristics of low-temperature geothermal waters issuing from carbonate reservoirs in the Çürüksu Graben within the eastern termination of the Büyük Menderes Graben in western Turkey. Temperatures and pH values of geothermal waters vary from 20.1 to 24.6 °C and 6.62 to 7.11 and those of cold waters are 17.1 to 19.9 °C and 6.85 to 7.72, respectively. Geothermal waters are of Ca-HCO_3 and Ca-SO_4 types whereas cold waters are characterized by these two types and Mg-HCO_3 as well. $\delta^{18}O$ and δD values of samples vary from −9.27‰ to −7.69‰ (VSMOW) and −58.06‰ to −52.2‰ and indicate a meteoric origin with local recharge. Tritium contents are from 0.12 to 2.17 TU for thermal waters and 0.28 to 4.85 TU for the cold waters implying relatively longer residence time for the hot waters. Thermal water samples mostly have positive $\delta^{13}C$ values (varying from −0.32‰ to +1.99‰) and carbon in these waters is likely derived from marine limestone or metamorphic CO_2. $\delta^{34}S$ and $\delta^{18}O$ values of dissolved sulfate in the waters indicate that sulfur originates from dissolution of marine evaporite deposits (e.g., gypsum). Çürüksu waters are generally oversaturated with respect to calcite, dolomite and quartz but undersaturated with respect to gypsum. Common ion effect exerted a strong control for the formation of travertine deposits in the area. Chemical and isotopic evaluations indicated that the diversity in the water chemistry of samples is attributed to a combination of processes including water-rock interaction, ion exchange and mixing of various types of waters. Çürüksu thermal waters are immature and not in chemical equilibrium with the reservoir rock. Among the various geothermometers applied to Çürüksu thermal waters, temperatures computed by chalcedony, quartz and Ca-Mg geothermometers are 21–52 °C, 49–83 °C and 73–96 °C, respectively. HCO_3-SO_4-F and anhydrite-chalcedony (quartz) diagrams estimated a temperature range of 63–86 °C and $\delta^{18}O(SO_4\text{-}H_2O)$ isotope geothermometer yielded 67–78 °C.

Key words: Water chemistry, isotope, geothermometry, mineral saturation, Çürüksu thermal waters

1. Introduction

Complex tectonomagmatic history of Turkey has resulted in widespread geothermal activity which manifests as many geothermal areas distributed through the country (Mutlu and Güleç, 1998). The General Directorate of Mineral Research and Exploration (MTA), the leading governmental actor in geothermal sector in Turkey, has drilled a number of 634 wells with total depth of 412,000 m. Nearly 5000 MWt heat energy is extracted from these wells where bottom-hole temperature is up to 287 °C. The current installed capacity of geothermal power in Turkey is around 1613 MWe (EPDK, 2021).

The convergence between the Eurasia and Africa plates has formed an extensive continental deformation in Anatolia giving rise to formation of several major tectonic structures such as the North and East Anatolian fault zones and the Aegean horst-graben system (Bozkurt, 2001). Most of high-temperature wells are in western Turkey, which also hosts a series of grabens such as the Büyük Menderes and Gediz and extensive Neogene volcanics. In this region, the crust is thin (Mc Kenzie, 1978) and heat flow values are above the global average (Cermac and Hurtig, 1979). Although Quaternary volcanism in the western Turkey is quite rare (localized only to Kula area), well-developed fault systems provide deep circulation for the fluids. High geothermal potential of western Anatolia has given rise to investigation of thermal fluids in various aspects including chemical and isotopic compositions, reservoir temperatures of hot waters (Şimşek, 1985; Mutlu and Güleç, 1998; Tarcan, 2005; Baba and Sözbilir, 2012; Alçiçek et al., 2018, 2019a, 2019b), and isotopic compositions of noble gases (Güleç et al,. 2002; Mutlu et al., 2008; Karakuş and Şimşek, 2013).

Most of the geothermal power plants have been established in the Büyük Menderes Graben (BMG) where the thermal fluids are produced through a number of

* Correspondence: agokgoz@pau.edu.tr

E-W extending normal faults. However, the temperature of geothermal fluids in the BMG decreases from Kızıldere towards east (Figure 1). The NW-SE extending Denizli Graben (DG) (also known as Çürüksu Graben, Çürüksu Basin or Denizli Basin and will be called as Çürüksu Graben in the oncoming parts), which is about 62-km-long and 7–28 km wide, in the eastern termination of BMG comprises a set of grabens and intervening horst blocks (Koçyiğit, 2005) (Figure 1).

The study area is located in the eastern limb of the Çürüksu Graben (ÇG) (Figure 1). Extensive distribution of Quaternary travertines not only in the ÇG but also throughout the BMG is an evidence of active tectonic extension and thermal water circulation. Although thermal fluids in almost all geothermal sites within the BMG have been the subject of intense research over the last three decades, low-temperature waters in the eastern part of ÇG have not been investigated. Therefore, the aim of this study is to discuss the geochemical evolution of the Çürüksu thermal waters on the basis of various water-rock interaction models. In addition, the reservoir temperature and the origin of waters and dissolved constituents were also examined using major element and stable isotope compositions.

2. Materials and method

A total of 27 water samples (hot and cold) were collected from 14 springs and 13 wells in the ÇG. The sample locations are shown in Figure 2. Temperature, electrical conductivity (EC) and pH values of waters were measured onsite by using Hach Lange HQ40D multiparameter. Before the measurements, the device was calibrated with

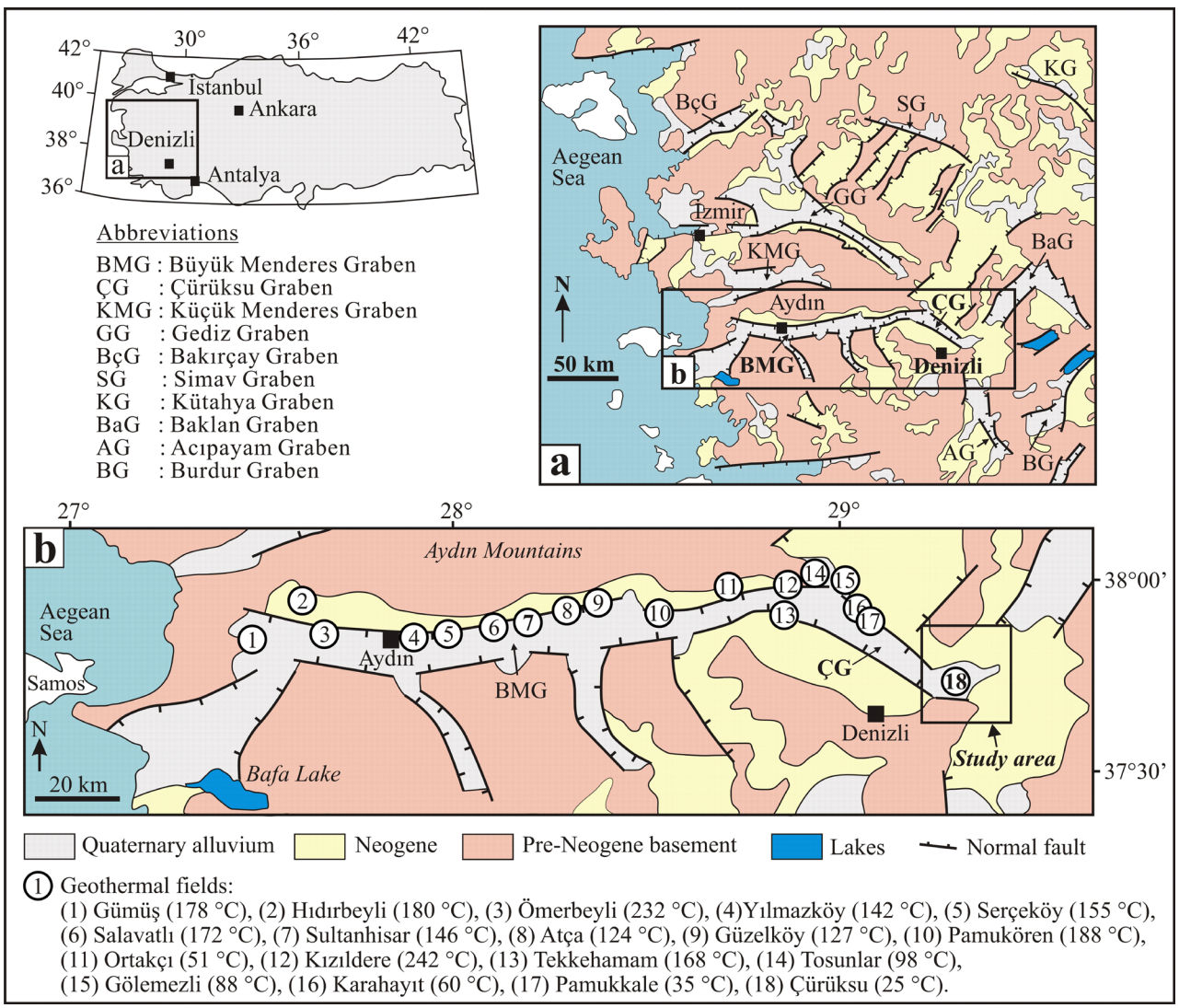

Figure 1. (a) General geological map of western Turkey (Bozkurt 2000). (b) Locations of major geothermal fields in the Büyük Menderes Graben (modified from Akkuş et al., 2005; Şimşek, 2005; Karakuş and Şimşek, 2013).

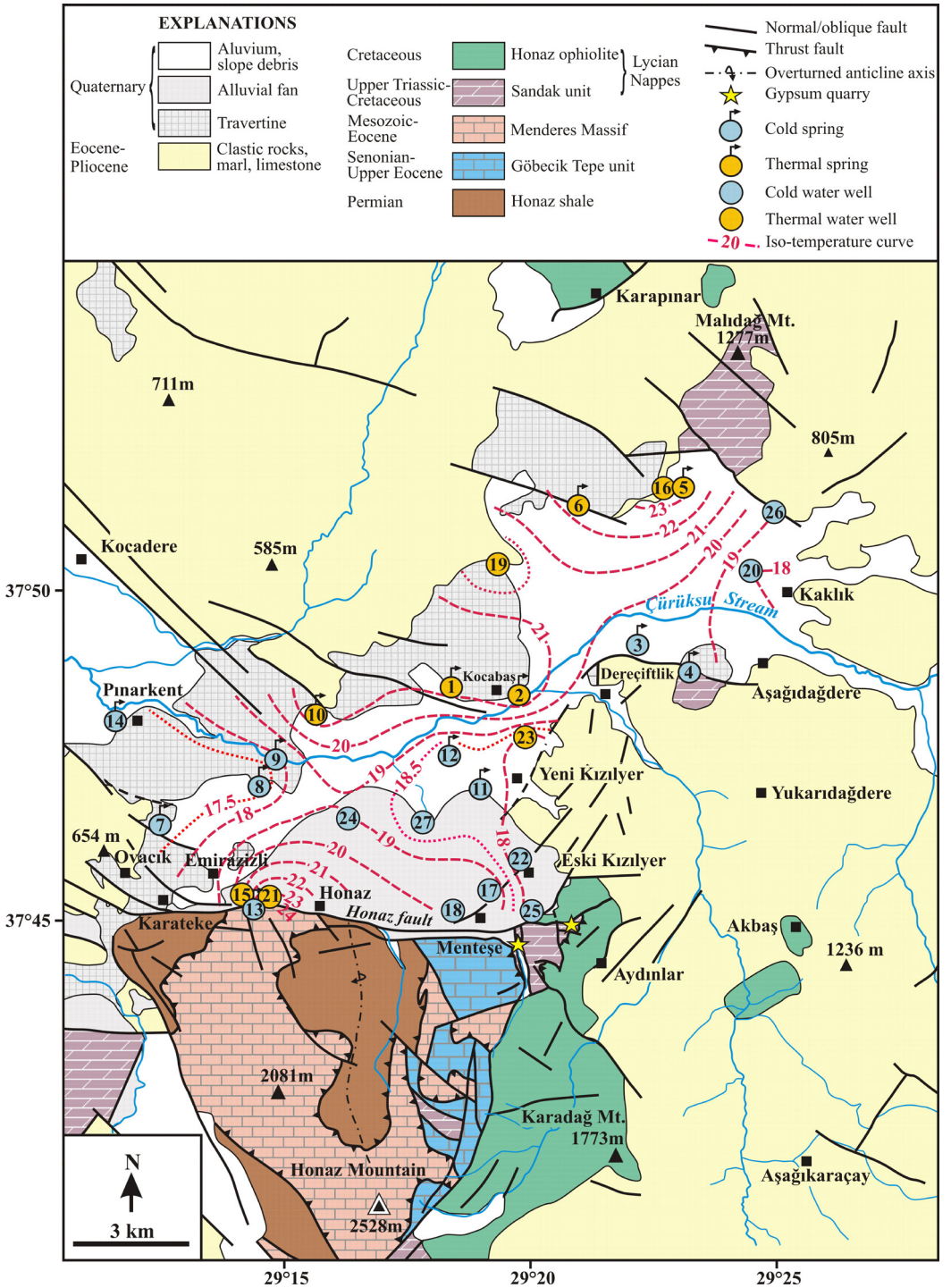

Figure 2. Geologic map of the study area (modified from Okay 1989; Bozkuş et al. 2001; Konak and Şenel 2002; Özkul et al. 2002; Emre et al. 2011) showing the location of sampled springs and wells.

standard solutions. Samples for ion analysis were taken into double-plugged 250-mL high-density polyethylene (HDPE) containers and filtered through 0.45 µm pore-size membranes. They were stored in cold chain (< +4 °C) until analysis. The batch taken for cation analysis was added concentrated ultrapure HNO_3 to lower pH to 2 or below. For $\delta^{18}O$-δD, $\delta^{34}S$ and $\delta^{13}C$ and tritium analyses, samples were taken into 50-mL and 100-mL and 500-mL HDPE

containers, respectively. For analysis of the $\delta^{34}S$ and $\delta^{18}O$ of the dissolved sulfate, water samples were collected by filtering into bottles of varying volumes (100 to 500 mL) depending on their sulfate concentrations. Then ultrapure HCl was added to keep the pH at 4–5. Finally, $BaSO_4$ was precipitated adding 100 to 150 mg of $BaCl_2.2H_2O$.

Major ion and tritium analyses of the waters were carried out at the Water Chemistry and Environmental Tritium Laboratory of the Hacettepe University by ion chromatography and the liquid scintillation counting method, respectively. Charge-balance error of waters is in the range of 1.9% to 4.8%. Silica analysis was made with spectrophotometric technique at the Geochemistry Laboratory of the Pamukkale University. HCO_3 concentrations were determined with H_2SO_4 titration using HACH microtitrator. Trace elements were analyzed at ACME laboratories by ICP-MS method with detection limit of 0.01 to 50 ppb. $\delta^{18}O$ and δD were measured with isotope ratio mass spectrometer at the SIRFER Laboratory of the University of Utah. Results with analytical precisions of 0.2‰ for $\delta^{18}O$ and 2‰ for $\delta^{2}H$ are reported relative to Vienna Standard Mean Ocean Water (VSMOW).

$\delta^{13}C$ (in dissolved inorganic carbon) and $\delta^{34}S$-$\delta^{18}O$ (dissolved sulfate) analyses were conducted at the Environmental Isotope Laboratory of the University of Waterloo with precision of 0.2‰ for $\delta^{13}C$ (VPDB), 0.3‰ for $\delta^{34}S$ (VCDT) and $\delta^{18}O$ (SMOW).

3. Geological and hydrogeological setting of study area

In the study area, the Permian Honaz Shale which is composed of slightly metamorphosed, dark bluish-green shale and siltstone comprises the bedrock (Okay, 1989; Konak and Şenel, 2002) (Figure 2). The unit exposing at the southwest of basin is locally cut by dark colored andesitic dykes. It is overlain by a tectonic contact by the Mesozoic-Eocene Menderes Massif metamorphites that are represented by gray, thick bedded, locally laminated recrystallized limestones, schist, calciturbidite and shale (Yılanlı and Zeybekölen Tepe formations: Okay, 1989). The massif in the area is overlain by Lycian nappes which are composed of Sandak Unit and the Honaz Ophiolite. Upper Triassic-Cretaceous Sandak Unit consists of massive thick bedded, dark gray-black colored dolomite and dolomitic limestone which are rarely alternated with thick gypsum layers (Okay, 1989). The Honaz Ophiolite of Cretaceous age which is the uppermost tectonic unit of the nappe sequence is composed of dark green, polished, blocky, partly serpentinized and silicified harzburgite accompanied by gabbro and chromite bodies (Okay, 1989; Gündoğan et al., 2008). Autochthonous limestone, conglomerate, sandstone and shale of Senonian-Upper Eocene Göbecik Tepe unit are overthrusted by the Menderes Massif in the eastern part of Honaz Mountain (Okay, 1989). Eocene-Pliocene deposits unconformably overlying all the older units (Figure 2) are comprised by conglomerate-sandstone-siltstone-claystone alternation and lacustrine limestones and mudstones interlayered with gypsum and coal levels and volcaniclastics. Quaternary travertine, alluvial fan, alluvium and slope waste cover all the underlying units.

The Mesozoic carbonate rocks in the ÇG have secondary porosity and permeability due to dissolution, faulting and fracturing and therefore, they form an important karst aquifer system. The Honaz fault defines a structural contact between recrystallized limestones of the Menderes Massif (Yılanlı Formation) and alluvial deposits. Slope waste with high clay content generates an impermeable-less permeable barrier for the groundwater that discharged northward across the recrystallized limestones. For this reason, springs of high-flow rate are manifested along the Honaz fault. In the study area, there are many springs issuing through the Mesozoic limestones, permeable Neogene units (limestone, conglomerate, and sandstone), travertines and the alluvial fan deposits. The average discharge of karstic springs (for the period of 1990–1993) is in the range of 14 to 1260 L/s (Özler, 1999). The area also hosts several water wells with depth up to 380 m (mostly 100–150 m). The majority of these wells, which are mostly of pumping type, were drilled on the alluvium. Groundwater flow is controlled by fracture systems and karstic spaces in the fissured karst aquifers (e.g., Menderes massif, Sandak and Göbecik Tepe Units) which are hydraulically connected to the porous aquifers. Especially the alluvial and travertine aquifers are replenished by infiltrating rainwater and by lateral recharge from the carbonate aquifers. The Çürüksu (means "rotten water" in Turkish) Graben has a significant groundwater potential. However, according to the Turkish Standard 266-Water Intended for Human Consumption (TS 266, 2005), only a few springs and well waters are potable and therefore most of the water is used for irrigation.

There is no recent volcanic activity in the region that can be a heat source for the thermal waters. According to Roche et al. (2019), the thermal anomaly in the Menderes Massif is closely related to the Hellenic subduction. Heat is conveyed from shallow asthenospheric mantle to the surface by fluid circulation through low-angle faults, and hence, the heat source of hydrothermal systems in the massif is originated from extensional tectonics rather than magmatism. Formun Üstü

Likewise, heat flow from lithospheric mantle due to large extension rate is suggested to play a critical role in the formation of Ortakçı geothermal field (Figure 1a, no. 11) and the heat transport is controlled by faults in a convection dominated system (Kaya, 2015).

Active faults, intense seismicity, alluvial fans, warm-water travertine deposits and low-temperature thermal waters are the manifestations of ongoing tectonic activity

in the ÇG. The Honaz fault with length of about 15 km is an active normal fault (Koçyiğit, 2005) and it bounds the basin in the south (Okay, 1989; Bozkuş et al., 2001; Koçyiğit, 2005; Özkaymak, 2015). It generated a number of earthquakes with magnitude up to 5.7 (Ms) (13.06.1965) and focal depths of 5 to 10 km (KOERİ, 2021).

İlkışık (1995) estimated the silica heat flow of low-temperature geothermal waters in ÇG in the range of 53 to 76 mW m^{-2}. The geothermal gradient map based on the estimation of the Curie point depths (CPDs) of western Turkey has shown that the geothermal gradient is about 60 °C/km around ÇG (Bilim et al., 2016). The ongoing seismic activity in the region has given rise to development of a number of normal faults and associated fracture systems. Warm groundwater discharging from these structural lines precipitated travertine deposits throughout the region (Figure 2). U-Th dating results of travertines indicate that tectonism in the region has been active for at least 600 ka (Claes et al., 2020).

The intensely fractured limestone, marble, calcschist, quartzschist and quartzite of the Menderes Massif are regarded as the major reservoir rocks in the Çürüksu area. Impermeable units of Neogene formations (siltstone, claystone and marl) comprise the cap rocks. The ÇG is recharged by meteoric waters infiltrating mainly through the carbonate rocks of the Menderes Massif, Göbecik Tepe and Sandak units, which are widely exposed on the Honaz, Çökelez (outside the study area) and Malı mountains and surrounding areas. The E-W, NW-SE and NE-SW trending faults and fracture sets are the main conduits for the emergence of thermal waters (Figure 2). Temperature of Çürüksu waters varies from 17.1 to 24.6 °C and it increases from the center of basin to the border faults at the south and north of the area (Figure 2). This clearly indicates that hot water circulation in the ÇG is controlled by faults and fracture systems.

4. Results

4.1 Water chemistry

Results of chemical analysis of Çürüksu water samples are given in Table 1. According to Bogomolov classification (Bogomolov and Silin-Bekcurin, 1955), studied waters with temperature between 20 and 37 °C are grouped as hypothermal waters. Based on this, eight samples (5 springs and 3 well waters) with temperature above 20 °C have been considered as thermal waters. pH values of waters are close to neutral falling in the range of 6.62 to 7.72. EC values vary in a wide range from 620 to 2080 µS/cm. Waters in the ÇG are divided into three categories with respect to their chemical composition:

(1) Ca-HCO_3 type waters of Group 1 have low EC (620–1012 µS/cm) and ion contents (except for HCO_3). They are represented by two thermal waters (wells 1 and 7) and three cold springs (Pınarbaşı, Kazanpınar and Böceli). (2) Mg-HCO_3 type waters of Group 2 comprise two well waters (wells 6 and 9). Well 12 with Mg-Ca-SO_4-HCO_3 type is also included to this group. Their EC values (918 and 1231 µS/cm) are higher than the first group. Except for Ca^{2+}, concentrations of Na^+, Mg^{2+}, Cl^- and SiO_2 exceed the Group 1. (3) Ca-SO_4 type waters of Group 3 include the majority of waters (6 thermal and 13 cold waters). They are characterized by relatively high EC values (891–2080 µS/cm) and Ca^{2+}, SO_4^{2-}, Sr and F^- contents. The average concentrations of Mg-HCO_3 type cold waters and Ca-HCO_3 and Ca-SO_4 type thermal and cold waters are illustrated in a semilogarithmic diagram (Figure 3). As shown in this graphic, Ca-HCO_3 type waters have similar concentration trends whereas ion contents of Ca-SO_4 type thermal waters are higher than their cold equivalents.

4.2 Isotope compositions

4.2.1 Oxygen and hydrogen isotope compositions of the waters

$\delta^{18}O$ and δD values of waters fall in the range of –9.27‰ to –7.69‰ (VSMOW) and –58.06‰ to –52.29‰ (VSMOW) (Table 2). These results are quite similar to isotope values of –9.11‰ to –8.55‰ and –59.46‰ to –53.92‰ measured for the karstic waters in the ÇG (Önhon et al., 1989). $\delta^{18}O$-δD isotope systematics of the waters differ only 1.6‰ and 5.8‰, respectively. In the $\delta^{18}O$ vs. δD diagram (Figure 4a), water samples are plotted between the Global (Craig, 1961) and Mediterranean (Gat and Carmi, 1970) Meteoric Water Lines that indicate a meteoric origin. It should be noted that waters from higher elevations are represented by lower $\delta^{18}O$ and δD values than those recharging at low altitudes.

Tritium values of samples are between 0.12 and 4.85 TU (Table 2). Tritium compositions of Ca-HCO_3 type cold waters are from 1.86 to 3.50 TU and those of thermal waters are measured between 1.26 (well 7) and 2.17 TU (well 1). Tritium contents of Ca-SO_4 type cold and thermal waters are 0.73–4.85 TU and 0.12–0.67 TU, respectively.

4.2.2. $\delta^{13}C$ composition

$\delta^{13}C$ values of water samples from the ÇG vary over a wide range from –9.52 to +2.88‰ (VPDB) (Table 2). $\delta^{13}C$ of Ca-HCO_3 type cold and thermal waters is –7.44‰ to –1.26‰ and –0.32‰ to +1.99‰, respectively. Among the Ca-SO_4 type cold waters, only the Kelkaya spring has a positive $\delta^{13}C$ value (+2.88‰ VPDB) and carbon isotope composition of other cold waters varies from –4.84‰ to –0.12‰. $\delta^{13}C$ of Ca-SO_4 type thermal waters is between +0.33‰ and +1.41‰. Mg-HCO_3 type waters are represented by the lowest $\delta^{13}C$ values ranging from –9.52‰ to –5.49‰.

4.2.3. $\delta^{34}S$-$\delta^{18}O$ (sulfate) compositions

To examine the source of sulfur and oxygen in dissolved sulfate in samples, $\delta^{34}S$ (SO_4) and $\delta^{18}O$ (SO_4) analyses were carried out (Table 2). $\delta^{34}S$ (SO_4) values of Ca-HCO_3 type waters are between 11.71‰ and 13.55‰ (VCDT) and

Table 1. Physicochemical properties and ion concentrations of studied waters (TS: Thermal spring, CS: Cold spring, TW: Thermal water well, CW: Cold water well).

No	Type	Name	T	EC	pH	Na^+	K^+	Ca^{2+}	Mg^{2+}	Cl^-	SO_4^{2-}	HCO_3^-	SiO_2	Li^+	B	Sr	F^-	NO_3^-	Water type
			(°C)	(µS/cm)		mg/L													
1	TS	Ağapınar	21.5	1964	6.78	31.7	3.85	380	120	20.0	914	500	26.97	0.087	0.49	7.78	1.59	3.0	Ca-Mg-SO_4-HCO_3
2	TS	Çayırlık	22.3	1892	6.93	39.7	4.36	322	124	29.8	784	511	30.89	0.085	0.46	6.89	1.44	2.3	Ca-Mg-SO_4-HCO_3
3	CS	Çamurlu	18.9	1715	6.90	17.6	3.18	258	145	10.1	698	517	62.79	0.106	0.61	5.95	1.35	2.8	Ca-Mg-SO_4-HCO_3
4	CS	Kelkaya	19.5	1890	7.01	20.4	3.56	349	91	10.9	623	656	22.37	0.130	0.70	6.02	1.50	0.3	Ca-Mg-SO_4-HCO_3
5	TS	İçgöl	23.4	1642	6.74	35.1	4.02	279	73	21.5	535	511	23.66	0.076	0.38	5.38	1.34	0.0	Ca-Mg-SO_4-HCO_3
6	TS	Kokarsu	22.4	1997	6.62	29.8	3.48	380	103	20.5	844	569	24.26	0.094	0.48	7.63	1.75	0.0	Ca-Mg-SO_4-HCO_3
7	CS	Kazanpınar	17.1	791	6.98	12.4	1.82	102	53	9.7	145	360	22.60	0.009	0.11	1.41	0.35	15.7	Ca-Mg-HCO_3-SO_4
8	CS	Dedepınar	17.1	891	7.15	17.9	2.86	141	56	16.2	261	331	19.12	0.010	0.07	2.13	0.45	15.7	Ca-Mg-SO_4-HCO_3
9	CS	Höyük	17.7	1102	7.10	13.4	2.54	193	75	5.9	462	320	21.24	0.014	0.09	3.16	0.52	9.3	Ca-Mg-SO_4-HCO_3
10	TS	Halkabaşı	21.9	2072	6.73	38.3	4.08	379	131	28.8	968	465	28.55	0.102	0.54	7.74	1.79	9.4	Ca-Mg-SO_4-HCO_3
11	CS.	Dandanaz	18.8	1494	7.31	6.5	1.36	283	106	4.8	867	227	36.17	0.008	0.04	9.72	1.43	6.7	Ca-Mg-SO_4
12	CS	Karakuş	17.9	1486	7.45	7.4	1.09	245	124	6.6	815	261	46.55	0.009	0.05	9.49	1.29	14.0	Ca-Mg-SO_4
13	CS	Pınarbaşı	19.6	620	7.35	7.0	0.99	89	38	4.3	110	290	12.13	0.008	0.04	1.09	0.35	2.5	Ca-Mg-HCO_3-SO_4
14	CS	Böceli	17.1	844	6.98	15.8	2.23	122	52	7.9	171	378	24.06	0.012	0.07	1.65	0.32	20.6	Ca-Mg-HCO_3-SO_4
15	TW	Well 1	20.1	750	7.11	9.4	1.23	120	40	4.4	125	378	13.31	0.012	0.07	1.21	0.40	2.0	Ca-Mg-HCO_3-SO_4
16	TW	Well 2	23.8	1953	6.77	33.6	4.21	368	112	21.3	793	575	24.61	0.090	0.44	6.80	1.66	0.0	Ca-Mg-SO_4-HCO_3
17	CW	Well 3	19.9	1437	7.05	8.0	1.58	291	90	4.2	747	290	18.77	0.024	0.12	5.21	1.03	0.8	Ca-Mg-SO_4-HCO_3
18	CW	Well 4	19.9	1340	7.72	8.1	1.24	255	74	4.1	637	273	16.89	0.025	0.12	4.71	0.89	0.0	Ca-Mg-SO_4-HCO_3
19	CW	Well 5	19.8	2080	6.85	35.5	4.38	396	134	21.4	1071	442	33.44	0.109	0.55	8.38	1.63	6.2	Ca-Mg-SO_4-HCO_3
20	CW	Well 6	18.0	918	7.62	40.3	1.67	50	95	21.9	147	425	42.15	0.010	0.20	0.55	0.15	20.9	Mg-Ca-HCO_3-SO_4
21	TW	Well 7	24.6	1012	6.66	17.8	2.42	158	55	5.3	178	523	15.48	0.033	0.18	1.68	0.61	0.0	Ca-Mg-HCO_3-SO_4
22	CW	Well 8	17.4	1414	7.32	6.7	1.64	276	101	4.6	814	203	41.73	0.007	0.04	9.23	1.69	2.4	Ca-Mg-SO_4
23	CW	Well 9	17.4	962	7.51	19.9	2.10	71	108	11.6	114	565	50.91	0.024	0.15	1.36	0.33	16.4	Mg-Ca-HCO_3
24	CW	Well 10	19.0	1282	7.08	16.9	1.56	212	74	6.0	511	320	22.55	0.020	0.10	4.29	0.80	6.3	Ca-Mg-SO_4-HCO_3
25	CW	Well 11	17.6	1437	7.21	5.8	0.85	296	92	4.3	839	232	19.05	0.007	0.03	9.13	1.55	1.3	Ca-Mg-SO_4
26	CW	Well 12	19.0	1231	7.32	20.7	2.11	78	158	21.8	368	459	64.80	0.026	0.22	2.03	0.29	30.4	Mg-Ca-SO_4-HCO_3
27	CW	Well 13	17.9	1359	7.13	9.1	1.47	251	83	5.3	658	285	23.10	0.020	0.16	5.12	1.00	3.7	Ca-Mg-SO_4-HCO_3

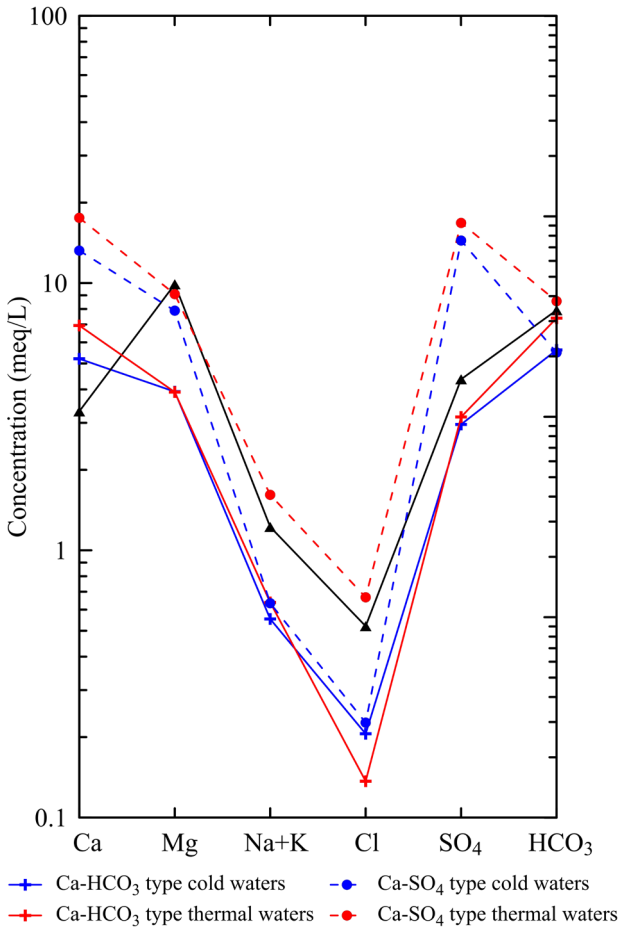

Figure 3. Semilogarithmic diagram (using the average concentrations of waters).

those of Ca-SO_4 type waters vary from 12.83‰ to 14.91‰ (VCDT). The lowest $\delta^{34}S$ is obtained from water of well 9 (8.07‰). $\delta^{18}O(SO_4)$ available for only four samples falls in a narrow range from 11.73‰ to 12.23 ‰ (VSMOW).

5. Discussion

5.1. Processes affecting the water chemistry

Molar Na^+/Cl^- ratio is a good indicator for the source of sodium in waters. If this ratio is close to one, halite dissolution is responsible for sodium concentration and if it is greater than one, silicate weathering reactions are the major source of sodium (Meybeck, 1987). In the Na^+ vs. Cl^- graphic (Figure 5a), there is a strong positive correlation between Na^+ and Cl^- (r = 0.932) and all waters plot to the left part of 1:1 line. Na^+/Cl^- ratio of Çürüksu waters varies from 1.47 to 5.18 (Table 3). Sodium excess in waters is also reflected by negative base-exchange index (BEI) values (from –5.45 to –0.94) (Table 3). Negative BEI values indicate the exchange of Ca^{2+} and Mg^{2+} with Na^+ and K^+ ions within the minerals. Such exchange reactions taking place in waters manifested from the Menderes Massif metamorphics result in Na^+ excess. Ion exchange occurring between groundwater and clay minerals that widely exist within Neogene units is another mechanism responsible for sodium excess in the Çürüksu waters.

Carbonate rocks in the study area are composed of limestone, dolomitic limestone and dolomite. They have an apparent thickness of more than 2000 m (Okay, 1989) and are widely exposed in the region. Carbonate weathering is the major source of Ca^{2+}, Mg^{2+} and HCO_3^- ions in the Çürüksu waters. Rainwater is slightly acidic due to dissolution of atmospheric carbon dioxide that forms

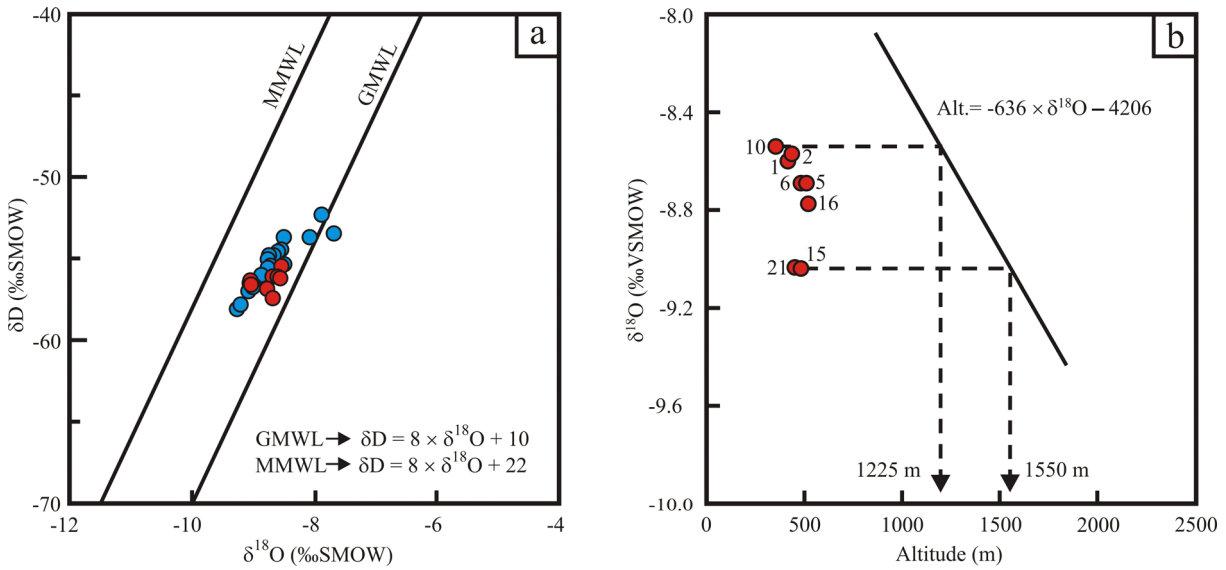

Figure 4. (a) $\delta^{18}O$ vs. δD diagram for the studied waters. Global Meteoric Water Line (GMWL) (Craig, 1961), Mediterranean Meteoric Water Line (MMWL) (Gat and Carmi, 1970). (b) Altitude vs. $\delta^{18}O$ diagram (regression equation was taken from Alçiçek et al., 2019b).

Table 2. Stable isotope (‰) and tritium compositions of waters.

No	Name	Altitude	$\delta^{18}O(H_2O)$	$\delta D(H_2O)$	D–exc	T (^3H)	$\delta^{18}O(SO_4)$	$\delta^{34}S(SO_4)$	$\delta^{13}C$
		(m)	(VSMOW)		(‰)	(TU)	(VSMOW)	(VCDT)	(VPDB)
1	Ağapınar	416	–8.60	–56.09	12.71	-	-	14.26	0.45
2	Çayırlık	436	–8.57	–56.16	12.40	-	-	-	-
3	Çamurlu	436	–8.73	–55.39	14.45	1.06 ± 0.25	-	-	-
4	Kelkaya	565	–8.77	–55.62	14.54	0.73 ± 0.24	-	14.29	2.88
5	İçgöl	511	–8.69	–57.37	12.15	0.67 ± 0.24	12.22	13.36	1.41
6	Kokarsu	483	–8.69	–56.08	13.44	0.12 ± 0.23	12.23	12.83	0.65
7	Kazanpınar	401	–8.60	–54.51	14.29	2.33 ± 0.26	-	11.82	–5.22
8	Dedepınar	377	–8.88	–55.95	15.09	-	-	-	-
9	Höyük	358	–8.98	–56.64	15.20	4.85 ± 0.31	-	13.25	–4.84
10	Halkabaşı	354	–8.54	–55.44	12.88	0.34 ± 0.24	11.73	14.37	0.33
11	Dandanaz	445	–8.66	–54.73	14.55	-	-	-	-
12	Karakuş	409	–8.55	–54.42	13.98	2.39 ± 0.25	-	-	-
13	Pınarbaşı	490	–9.06	–56.47	16.01	1.86 ± 0.40	-	13.21	–1.26
14	Böceli	310	–8.50	–53.67	14.33	3.50 ± 0.26	-	11.71	–7.44
15	Well 1	487	–9.05	–56.31	16.09	2.17 ± 0.40	-	-	–0.32
16	Well 2	513	–8.78	–56.80	13.44	-	-	-	-
17	Well 3	583	–9.20	–57.79	15.81	2.97 ± 0.26	-	-	-
18	Well 4	525	–9.27	–58.06	16.10	3.73 ± 0.27	-	14.91	–0.12
19	Well 5	471	–8.50	–55.32	12.68	-	-	14.43	–0.15
20	Well 6	531	–7.69	–53.43	8.09	0.28 ± 0.24	-	=	–9.52
21	Well 7	470	–9.04	–56.57	15.75	1.26 ± 0.39	12.02	13.55	1.99
22	Well 8	533	–8.75	–54.96	15.04	-	-	-	-
23	Well 9	444	–7.88	–52.29	10.75	-	-	8.07	–9.00
24	Well 10	431	–9.01	–56.72	15.36	4.40 ± 0.28	-	14.00	–3.30
25	Well 11	624	–8.74	–54.77	15.15	2.14 ± 0.25	-	-	-
26	Well 12	553	–8.08	–53.66	10.98	-	-	14.62	–5.49
27	Well 13	447	–9.08	–56.96	15.68	-	-	-	-

-: not analyzed.

weak carbonic acid (H_2CO_3). Interaction of CO_2-rich rainwater with the carbonate rocks dissolves Ca^{2+}, Mg^{2+} and HCO_3^- through the weathering reactions:

Limestone dissolution:

$$CaCO_3 + H_2O + CO_2 \rightarrow Ca^{2+} + 2HCO_3^- \quad (1)$$

Dolomite dissolution:

$$CaMg(CO_3)_2 + 2H_2O + 2CO_2 \rightarrow Ca^{2+} + Mg^{2+} + 4HCO_3^- \quad (2)$$

Molar Ca^{2+}/Mg^{2+} ratio in waters is a perfect indicator for the type of carbonate rock dissolved. For example, Ca^{2+}/Mg^{2+} ratio close to one implies dolomite dissolution whereas higher values indicate dissolution of calcite mineral (Mayo and Loucks, 1995). Ca^{2+}/Mg^{2+} ratios are 0.32, 0.39 and 0.30 for the waters of wells 6, 9 and 12. Ca^{2+}/Mg^{2+} ratio for other samples varies between 1.07 and 2.30 (Table 3). In the Ca^{2+} vs. Mg^{2+} diagram, except for samples with low Ca^{2+}/Mg^{2+} ratio, all the waters plot to the right part of (under) 1:1 line indicating a Ca-rich source rock (Figure 5b). Molar Ca^{2+}/HCO_3^- ratio of waters is from 0.43 to 2.07. In the Ca^{2+} vs. HCO_3^- graphic (Figure 5c), 05:1 line indicates that limestone (calcite) weathering is the major source of Ca^{2+} and HCO_3^- ions. Thermal (samples 15 and 21) and cold (samples 7, 13 and 14) waters plotting on this

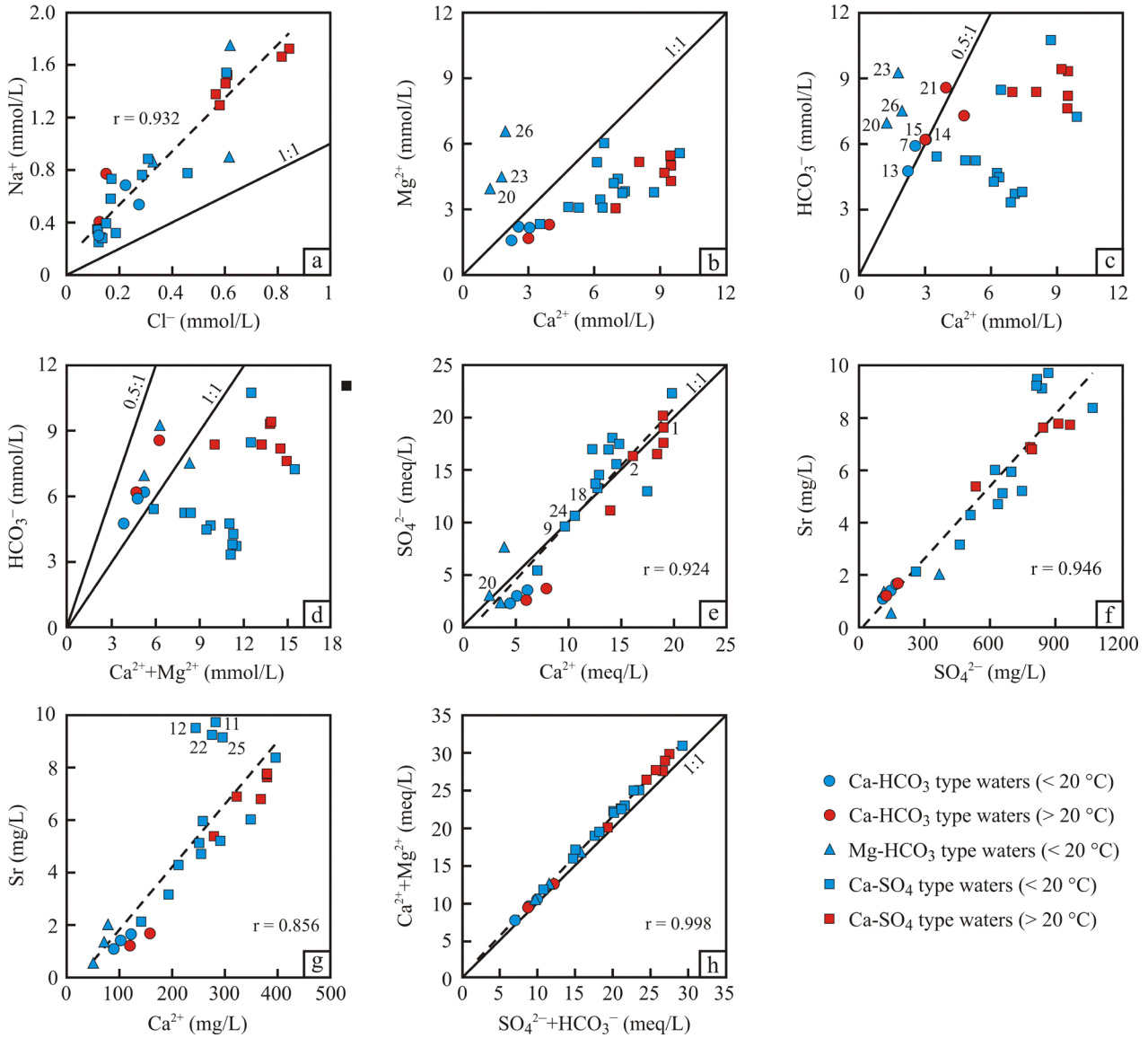

Figure 5. Variations in element contents for the waters in the ÇG. Dashed line is the regression line.

line are located close to the Honaz fault and manifested from the karstic limestones of the Yılanlı Formation. $(Ca^{2+}+Mg^{2+})/HCO_3^-$ ratios of waters fall in the range of 0.68 to 3.34. In the $(Ca^{2+}+Mg^{2+})$ vs. HCO_3^- graphic (Figure 5d), Ca-HCO_3 (Group 1) and Mg-HCO_3 (Group 2) type waters plot between 0.5:1 and 1:1 lines. As shown in the Figures 5b and c, there is an Mg^{2+} excess in well waters 6, 9 and 12 (samples 20, 23 and 26). In well 9, clay units were cut in the first 57 m and then conglomerate was encountered at depths of 57–141 m. The conglomerate is composed dominantly of peridotite clasts, and therefore, dissolution of ultramafic rock (particularly serpentinite) controls the water chemistry of this well by the reaction of:

$$Mg_3Si_2O_5(OH)_4 + 6CO_2 + 5H_2O \rightarrow 3Mg^{2+} + 6HCO_3^- + 2H_4SiO_4 \quad (3)$$

This reaction explains the Mg^{2+} excess in waters. Although no information is available for the rock type of conglomerate clasts in other wells, they might have similar lithology and water chemistry with well 9. However, water of well 6 contains two-fold Na^+ and SiO_2 and less Ca^{2+} in

Table 3. Molar ratios of ions and base-exchange indices (BEI) of the water samples.

No	Name	Na^+/Cl^-	Ca^{2+}/Mg^{2+}	Ca^{2+}/HCO_3^-	$Ca^{2+}+Mg^{2+}/HCO_3^-$	Ca^{2+}/SO_4^{2-}	BEI*
1	Ağapınar	2.45	1.90	1.16	1.77	1.00	–2.06
2	Çayırlık	2.06	1.56	0.96	1.58	0.99	–1.35
3	Çamurlu	2.69	1.07	0.76	1.47	0.89	–2.69
4	Kelkaya	2.89	2.30	0.81	1.16	1.34	–2.88
5	İçgöl	2.52	2.29	0.83	1.20	1.25	–2.08
6	Kokarsu	2.24	2.21	1.02	1.48	1.08	–1.82
7	Kazanpınar	1.97	1.15	0.43	0.81	1.69	–1.87
8	Dedepınar	1.71	1.51	0.65	1.08	1.30	–1.41
9	Höyük	3.51	1.54	0.92	1.52	1.00	–3.73
10	Halkabaşı	2.05	1.74	1.24	1.96	0.94	–1.37
11	Dandanaz	2.09	1.60	1.90	3.09	0.78	–2.21
12	Karakuş	1.73	1.19	1.43	2.64	0.72	–1.69
13	Pınarbaşı	2.51	1.41	0.47	0.80	1.94	–2.60
14	Böceli	3.09	1.41	0.49	0.84	1.71	–3.12
15	20019	3.30	1.80	0.48	0.75	2.30	–3.43
16	33278	2.44	1.97	0.98	1.47	1.11	–2.01
17	37265	2.94	1.94	1.53	2.32	0.94	–3.16
18	37266	3.05	2.07	1.42	2.11	0.96	–3.21
19	39334	2.56	1.77	1.37	2.14	0.89	–2.14
20	43530	2.84	0.32	0.18	0.75	0.82	–2.29
21	44153	5.18	1.72	0.46	0.73	2.13	–5.45
22	44180	2.25	1.64	2.07	3.34	0.81	–2.44
23	46978	2.65	0.39	0.19	0.68	1.50	–2.48
24	49467	4.35	1.72	1.01	1.60	1.00	–4.41
25	52873	2.08	1.93	1.95	2.95	0.85	–2.14
26	55136	1.47	0.30	0.26	1.13	0.51	–0.94
27	63029	2.65	1.81	1.34	2.08	0.92	–2.75

* BEI = (Cl – (Na + K) / Cl); (Schoeller, 1934).

comparison to other two wells, which is possibly attributed to the ion exchange process. Groundwater circulation at shallow depths dissolves the serpentinized peridotites of Honaz Ophiolite and releases Mg^{2+} and HCO_3^-. Flow of this water into the karstic carbonate aquifers results in, to a certain extent, Mg^{2+} and HCO_3^- enrichment of groundwater in the aquifer.

Ca^{2+} excess recognized in most of waters (Figures 5b–5d) might indicate Ca^{2+} is derived from another source rather than carbonate weathering since most of samples do not follow the $Ca^{2+}/HCO_3^- = 1$ line typical of dissolution of carbonate rocks (Figure 5c). Gypsum at the layer surface of Mesozoic limestones (carbon associated sulfur: CAS, Kampschulte and Strauss, 2004), gypsum deposits (currently mined) within dolomites of the Sandak Unit and the gypsum levels within Neogene units are the other sources of Ca^{2+}. Gypsum hosted in these units is easily dissolved by groundwater and Ca^{2+} and SO_4^{2-} ions are released to the water:

$$CaSO_4.2H_2O + H_2O \rightarrow Ca^{2+} + SO_4^{2-} + 3H_2O \quad (4)$$

Molar Ca^{2+}/SO_4^{2-} ratio of waters varies from 0.51 to 2.30 (Table 4). Ca^{2+} vs. SO_4^{2-} graphic shows that there is a strong positive correlation between Ca^{2+} and SO_4^{2-} ($r = 0.924$) and most of Ca-SO_4 type waters (Group 3) plot on or near 1:1 line (Figure 5e). This indicates that dissolution of gypsum is the major mechanism for the source of Ca^{2+} and SO_4^{2-} in waters (Table 3; Figure 5e). The majority of evaporate minerals in the Sandak Unit are composed of secondary

Table 4. Reservoir temperatures (°C) obtained with chemical and isotopic geothermometers.

Geothermometer	Calibration	Ağapınar	Çayırlık	İçgöl	Kokarsu	Halkabaşı	Well 1	Well 2	Well 7	Mean
$T_{measured}$		21.5	22.3	23.4	22.4	21.9	20.1	23.8	24.6	
Chalcedony	Fournier (1977)	43	49	38	39	46	-	40	-	43
Chalcedony	Arnorsson et al. (1983)	46	52	41	42	49	21	43	26	43
Quartz	Fournier (1977)	75	81	70	71	77	49	71	54	69
Quartz	Arnorsson et al. (1983)	78	83	73	74	80	54	75	59	72
Li	Fouillac and Michard (1981)	83	82	80	85	87	41	84	61	75
Ca-Mg	Chiodini et al. (1995)	84	73	96	93	78	85	86	81	85
$^{18}O(SO_4-H_2O)$	Lloyd (1968)	n.a.	n.a.	77	77	81	n.a.	n.a.	76	78
$^{18}O(SO_4-H_2O)$	Mizutani and Rafter (1969)	n.a.	n.a.	66	66	71	n.a.	n.a.	65	67
$^{18}O(SO_4-H_2O)$	Halas and Pluta (2000)	n.a.	n.a.	27	27	31	n.a.	n.a.	27	28
$^{18}O(SO_4-H_2O)$	Zeebe (2010)	n.a.	n.a.	34	34	38	n.a.	n.a.	33	35

n.a.: not analyzed, -: values lower than measured temperature.

gypsum (after anhydrite) accompanied by dolomite ($CaMg(CO_3)_2$), magnesite ($MgCO_3$), celestite ($SrSO_4$), and secondary calcite (Gündoğan et al., 2008). The strong correlation between Sr and SO_4^{2-} (r = 0.946: Figure 5f) might imply that celestite ($SrSO_4$) dissolution contributes strontium to the waters. This is also supported by the Ca^{2+} vs. Sr diagram (Figure 5g). If Ca^{2+}, Mg^{2+}, HCO_3^- and SO_4^{2-} are derived from simple dissolution of limestone (calcite), dolomite and gypsum, ($Ca^{2+}+Mg^{2+}$) and ($SO_4^{2-}+HCO_3^-$) should be correlated at a ratio of around 1:1 (McLean et al., 2000). In the ($Ca^{2+}+Mg^{2+}$) vs. ($SO_4^{2-}+HCO_3^-$) diagram, there is a strong positive correlation between these two ion pairs (r = 0.998) and studied waters plot very close to the 1:1 line (Figure 5h). Considering the mineral composition of aquifer lithologies in the area, it is suggested that water chemistry is chiefly defined by carbonate and gypsum dissolution. Silicate weathering and ion exchange reactions also contributed to the variations in Ca^{2+}, Mg^{2+}, HCO_3^-, Na^+ and SiO_2 concentrations.

Ca-SO_4 type thermal waters are slightly acidic and their Na^+, Cl^-, Li^+ and B concentrations are somewhat higher than the cold waters (Table 1). Ion concentrations of Ca-HCO_3 type thermal waters are relatively low and their chemical composition is similar to Ca-HCO_3 type cold waters (Figure 3). Ion concentration vs. temperature diagrams for some of Ca-HCO_3 type waters (Pınarbaşı spring, wells 1 and 7) are shown in Figures 6a and 6b. Among the Ca-HCO_3 type waters, Pınarbaşı spring has the lowest temperature value and ion concentration. As the temperature increases (from 19.6 to 24.6 °C), concentrations of Ca^{2+}, Mg^{2+}, Cl^-, HCO_3^-, SO_4^{2-} and SiO_2 also increase. The maximum increase occurred in Na^+ and HCO_3^- concentrations. B, F^- and Li^+ contents of these waters are also increased within the analytical error (Table 1). Well 7 with a depth of 150 m is an artesian type well and discharges the highest-temperature water. In this well, compact, firm, fractured limestone of the Menderes Massif (Yılanlı Formation) comprises the depths of 72–150 m. The geothermal fluid rising through the active Honaz fault at the south of ÇG is mixed with groundwater in the karstic aquifer which modifies the temperature and chemical composition of water.

In the light of the foregoing findings, processes influencing the chemical composition of Çürüksu waters include water-rock interaction (carbonate dissolution and precipitation, gypsum dissolution, silicate weathering), ion exchange, mixing of various types of groundwaters and combination of these processes.

5.2. Isotopic composition of waters

5.2.1. ^{18}O, D and tritium

Stable isotopes of oxygen ($\delta^{18}O$) and deuterium (δ^2H) are powerful tools to investigate the origin (e.g., meteoric, fossil and metamorphic) and recharge area of geothermal waters and temperature of reservoir water. Isotope compositions of precipitation (snow or rainwater) are the major input for the assessment of isotopic evolution of groundwater (Craig, 1961). Differences in the isotopic composition of rainwater are related to condensation process that take place under varying temperatures during the movement of water vapor within the atmosphere (Clark and Fritz, 1997).

Limited data are available for the isotope composition of rainfall around the Denizli region. $\delta^{18}O$ and δD values reported by the State Hydraulic Works (DSI) are –7.7‰ to –6.8‰ and –54.6‰ to –21.9‰ (Önhon et al., 1989). The data covering the Honaz area (1986–1987 period) are not sufficient to make a reliable assessment. Almost a

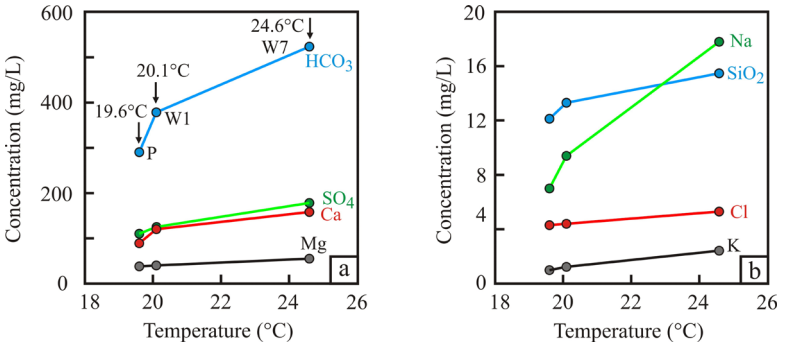

Figure 6. Ion concentration vs. temperature diagrams for some of Ca-HCO_3 type waters (P: Pınarbaşı, W1: well 1, W7: well 7).

decade ago, DSI carried out a stable-isotope survey on the rainfall of the Antalya city (165 km from Çürüksu) which revealed $\delta^{18}O$ of –12.1‰ to +2.1‰ (average –4.7‰) and δD of –73.5‰ to +17.1‰ (average –22.3‰). Based on these values, the equation of Antalya Meteoric Water Line is estimated $\delta D = 8 \text{ ´ } \delta^{18}O + 17.68$ (Dilaver et al., 2018). Since the isotope fractionation between water and vapor is more significant at lower temperatures, vapor moving to cold inland areas at the higher elevations is gradually depleted in heavy isotopes. Air masses transferring from the Mediterranean Sea to the Denizli region have much negative isotope values (enriched in light isotopes) as they rise to higher altitudes and colder regions. Repeated rainfalls also result in isotopic ratios of the air mass decrease inland (Kendall et al., 1995). The annual average atmospheric temperature in the city of Denizli is lower than Antalya. Groundwater in the Çürüksu area is mostly recharged by the rainfall from the Honaz Mountain (2528 m), which well explains the low $\delta^{18}O$ and δD values of precipitation in Denizli region.

In the study area, short-term hydrological surveys were conducted on spring waters of the ÇG. Results of $\delta^{18}O$ and δD analyses reported for the years of 1986–1987 are –9.26‰ to –8.29‰ and –59.12‰ to –50.04‰, respectively (Önhon et al., 1989). In another study by Özler (2000), $\delta^{18}O$ and δD values are given –9.11‰ to –8.55‰ and –59.46‰ to –53.92‰. Stable isotope compositions of the Çürüksu waters reported in these studies are consistent with our results. Deuterium excess of waters is between 8.1‰ and 16.1‰ (average 14‰, median 14.4‰) implying that waters are originated from the Mediterranean moisture (Table 2). We suggest that isotopic composition of Çürüksu waters have become slightly positive than the initial values due to mixing with thermal fluids and evaporation during precipitation and runoff.

In order to compute the recharge altitude of the waters in the ÇG, either the stable isotope ($\delta^{18}O$, δD) values of the annual precipitation or the springs recorded at different elevations must be known. However, there is no data on the $\delta^{18}O$ and δD composition of rainfall and spring waters in the region. Therefore, we used the equations of Alçiçek et al. (2019b) (altitude (m) = –636 x $\delta^{18}O$ – 4206) and (altitude (m) = –152 x δD – 7171) which are proposed for the Pamukkale geothermal field. Recharge altitudes for the Çürüksu waters estimated by the $\delta^{18}O$ and δD equations are 685 to 2141 m and 777 to 2163 m, respectively. Recharge zone of thermal waters is represented by a narrow range of altitude between 1225 and 1550 m (Figure 4b). The computed altitudes indicate that studied waters are recharged from the flanks of Honaz Mountain at the south and Malı (1277 m) and Çökelez (1840 m) mountains to the north.

In the Piper diagram (Figure 7), temperatures, $\delta^{18}O$ values and chemical compositions of thermal waters in the eastern part of the BMG are compared. High-temperature geothermal waters are enriched in ^{18}O as a result of water–rock interaction (particularly carbonate lithology). In geothermal waters, magnitude of the ^{18}O enrichment (also known as the oxygen isotope shift) is an indicator for high reservoir temperatures and/or increasing residence times. For the Kızıldere waters which have the highest bottom-hole temperature (242 °C) in BMG, isotope composition shift from the local meteoric line is 3.0‰ to 4.0‰ (Karakuş and Şimşek, 2013). The degree of $\delta^{18}O$ shift gradually decreases from Kızıldere field towards the Tekkehamam, Gölemezli, and Pamukkale-Karahayıt geothermal waters. $\delta^{18}O$ shift in the thermal waters of the ÇG is not significant (Figure 4a). Chemical composition of waters varies from Na-HCO_3 type which points to a high-temperature water-rock interaction within the Menderes Massif metamorphics at Kızıldere to Ca-Mg-SO_4-HCO_3 type standing for a low-temperature carbonate reservoir in the ÇG. The chemistry of reservoir waters in these geothermal fields is modified by mineralogical composition of reservoir rocks, temperature, reservoir depth and mixing with cold groundwater. H_2S or SO_2 significantly modify

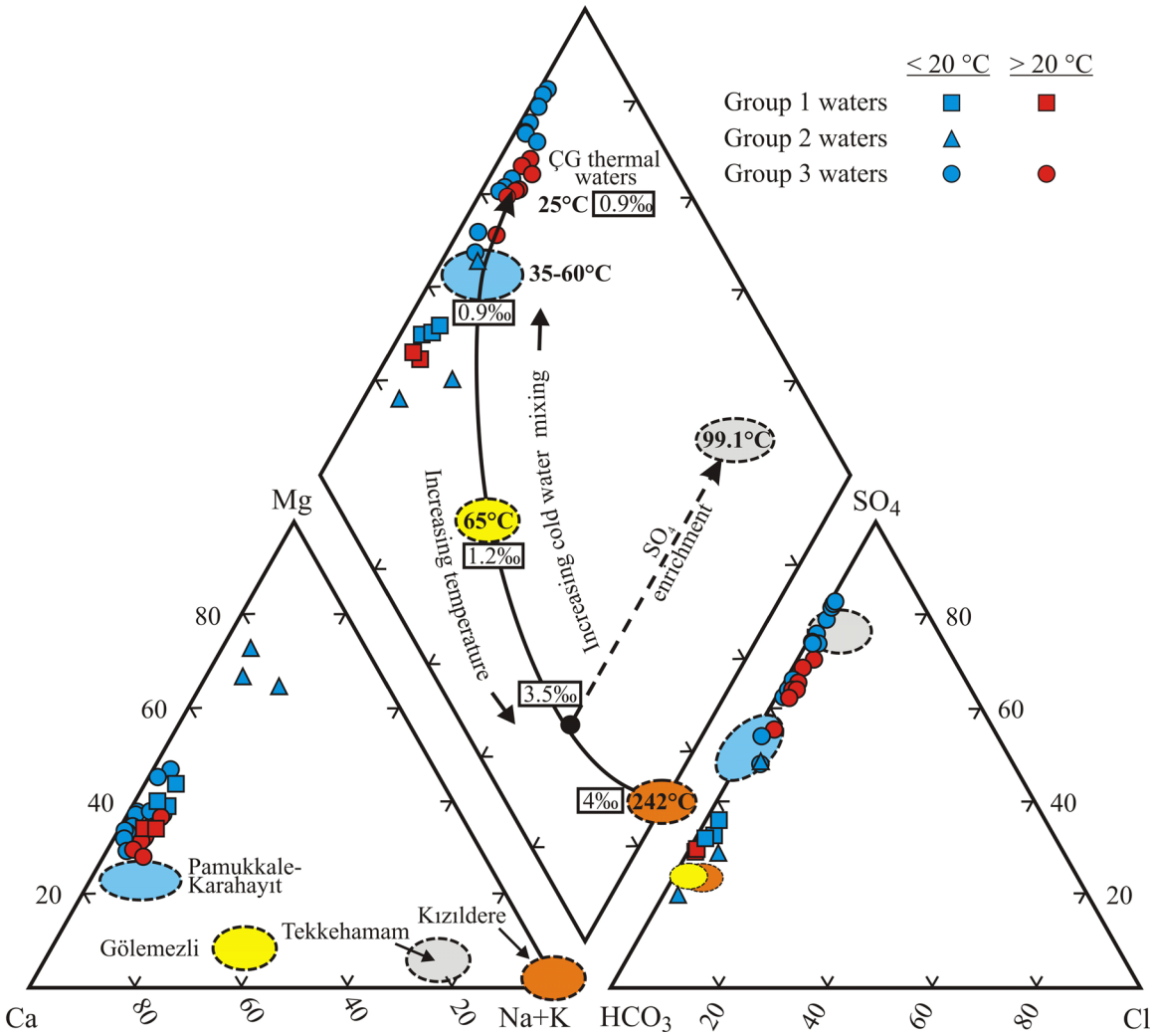

Figure 7. Piper diagram for thermal waters in eastern part of the BMG. Red and white circles represent for thermal and cold waters in the study area, respectively. Numbers in boxes and ellipses are oxygen isotope ($\delta^{18}O$) and temperature values of waters. The chemical and isotopic compositions of the waters in other areas were taken from Şimşek (2003) for Kızıldere, Kele et al. (2011 and Özkul et al. (2013) for Pamukkale, Avşar and Altuntaş (2017) for Tekkehamam, Alçiçek (2018) for Gölemezli and Alçiçek (2019a) for Karahayıt. See Figure 1b for locations of geothermal fields.

the chemical composition of Na-SO_4 type Tekkehamam thermal waters (Karakuş and Şimşek, 2013). Wells in these fields cut the Menderes Massif metamorphics at 530–1050 m in Kızıldere, 820 m in Tekkehamam, 407–640 m in Gölemezli and 60–315 m in Karahayıt (Akkuş et al., 2005). This shows that reservoir depth and cap rock thickness decrease from west to the east in the area of these wells.

Tritium (^3H) which is a radioactive isotope of hydrogen with a short half life (12.32 years; Lucas and Unterweger, 2000) decays to ^3He. Tritium count values is given in Tritium Units (TU). 1 TU is equal to 1 tritium atom per 10^{18} hydrogen atoms (Evans, 1996). Therefore, it is helpful to estimate the residence time of waters (Clark and Fritz, 1997). Tritium concentrations are high for shallow-circulating water and low (generally close to zero) for deep circulating waters.

During monthly measurements (1986–1987 years) in Honaz by DSI, tritium values of precipitation were found in the range of 6 to 30 TU (Önhon et al., 1989). For the same period, tritium values of studied waters were measured 0 to 11 TU and those in 1993 were recorded 0 to 7 TU (Özler, 1999). Because weighted annual data are not available for the study area, an approach was made here for tritium contribution from the precipitation. Tritium value of Honaz rainfall in November 2017 was 5.64 TU and ^3H concentration (May 2018) of a dilute spring (Kızılpınar spring) issuing at an elevation of 1408 m at north of the Honaz Mountain is reported 5.11 TU

(Semerci, 2019). Since spring waters at higher elevations record time wise tritium variations, they might reflect cumulative (or less than) tritium concentration of the rainfall. Tritium compositions of 0.12 to 1.06 TU measured in the Çamurlu, Kelkaya, İçgöl, Kokarsu and Halkabaşı spring waters and well 6 yield a residence time of more than 60 years. Higher tritium values of other waters imply a short circulation period and recharge by modern rainfall. In Figure 8, tritium contents of samples are compared to chloride that behaves conservatively in waters. It is shown that, except for two waters, most samples with relatively higher temperature are plotted in the area with higher Cl and lower tritium contents. However, the majority of cold waters with varying tritium contents plot to the left part of the diagram. Halkabaşı spring (sample no 10) with the highest Cl and low tritium contents probably represents the deep water circulation in the ÇG.

5.2.2. ^{13}C composition of the waters

CO_2 formed by the decay of organic matter in soil and by the dissolution of carbonate rocks and, magmatic and atmospheric CO_2 (although rare) are the principal sources of carbon in waters. Carbon isotope composition of these different carbon inputs is also variable. For example, $\delta^{13}C$ of marine limestones is between –3‰ and +3‰ but is much negative (from –6‰ to –7‰) for the atmospheric CO_2 (Clark and Fritz, 1997). Since organisms consume light isotope of carbon (^{12}C), carbon of organic origin may have extremely negative $\delta^{13}C$ value (e.g., –50‰).

$\delta^{13}C$ (DIC–dissolved inorganic carbon) values of Çürüksu waters are between –9.52‰ and +2.88‰. Samples with temperature of > 20 °C mostly have positive $\delta^{13}C$ and carbon in these waters is likely derived from marine limestone or metamorphic CO_2. The negative carbon isotope values recorded in the **Çürüksu** waters may be attributed to an organic source (e.g., biogenic soil, CO_2: –12‰) or atmospheric carbon dioxide. $\delta^{13}C$ of some cold waters is consistent with marine limestones. However, carbon isotope composition of well 7 and Kelkaya spring corresponds to metamorphosed carbonate rocks. Strontium and stable isotope ($\delta^{13}C$= –3.8‰ to +2.6‰) data on the Ballık travertines are indicative of a mixing between heavy-carbon rich, hypogene type paleofluids and light-carbon rich, shallowly circulated fluids (Claes et al., 2015). For this reason, travertines in the study area might be regarded as endogenic type, which were deposited from a deeply circulated fluid with varying temperature (Crossey et al., 2006).

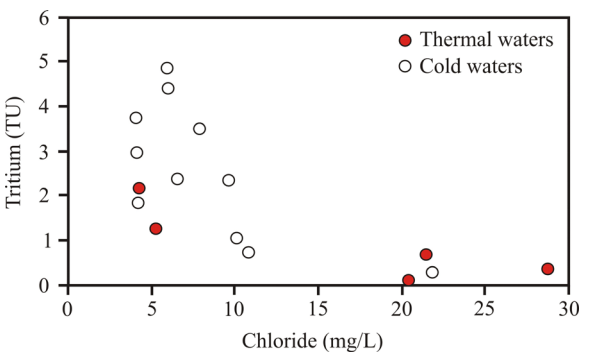

Figure 8. Tritium vs. chloride diagram for the studied waters.

Carbon isotope systematics of geothermal fluids in western Anatolia, particularly BMG, has been investigated in a number of studies. $\delta^{13}C$ (DIC) values of fluids for the Karahayıt area are 5.92‰ to 9.02‰ (Alçiçek et al., 2019a) and for the Gölemezli and Pamukkale geothermal fields in the eastern part of BMG are 6.26‰ to 8.07‰ (Alçiçek et al., 2018, 2019b). These values are generally higher than our results.

Karakuş and Şimşek (2013) and Mutlu et al. (2008) measured $\delta^{13}C$ (CO_2) (VPDB) in several geothermal fields in the same graben in the range of –5.39‰ to 0.02‰ and –2.35‰ to -0.62‰, respectively. These ratios are significantly lower than $\delta^{13}C$ of (DIC) in thermal waters of the western Anatolia. This is due to enrichment of light carbon isotope (^{12}C) in the gas phase during CO_2 removal from the waters (e.g., Mutlu et al., 2012).

An attempt is made here to estimate $\delta^{13}C_{CO2}$ from $\delta^{13}C$ values of several Quaternary travertine deposits around the ÇG (Özkul et al., 2013). In the calculations, we used the empirical equation of [$\delta^{13}C_{CO2}$ = 1.2 ´ $\delta^{13}C_{Trav.}$ – 10.5] proposed by Panichi and Tongiorgi (1976). Computation yielded $\delta^{13}C_{CO2}$ values varying from –15.3‰ to –3.5‰ (VPDB) which are within the range of $\delta^{13}C$ (CO_2) measured in geothermal fluids in the study area (Mutlu et al., 2008; Karakuş and Şimşek, 2013) but lower than the majority of $\delta^{13}C$ (DIC) values reported in this study. In fact, computed $\delta^{13}C$ (CO_2) values match with the mantle array (about –6.5‰). Previous studies (e.g., Güleç et al., 2002; Karakuş and Şimşek, 2013) around the study area indicated significant amount of mantle–He (almost approximately 45% of the total helium inventory) in the thermal fluids accompanied by high CO_2 concentrations. This high carbon flux is probably derived from marbles of the Menderes Massif metamorphics that comprise the basement lithology in most parts of the western Anatolia. Transfer of these volatiles (He and CO_2) to the crust is probably associated with fluid degassing from mantle melts that were generated by current extension in the region (Mutlu et al., 2008).

5.2.3 ^{34}S composition of the waters

Since sulfur has a variety of oxidation states (–2 to +6), $\delta^{34}S$ ratios of geologic materials vary in a wide range from –50‰ to +50‰ (Krouse and Mayer, 2000; Izbicki et al., 2005). Sulfate in waters is derived from multiple sources. Dissolution of sulfate minerals (e.g., gypsum), oxidation of sulfide minerals (e.g., pyrite) and biological activity are the major sulfate reservoirs. Modern seawater which

is another sulfate source has a homogeneous $\delta^{34}S$ value of +20‰ (Krouse, 1976). $\delta^{34}S$ (SO_4) of marine sediments is highly variable with respect to timing of deposition, ranging from +10‰ to +30‰ for Paleozoic and Mesozoic and +20‰ for the Tertiary deposits. Magmatic sulfur is represented by a narrow range of $\delta^{34}S$ between +5‰ and –5‰ (Clark and Fritz, 1997). On the other hand, sulfur reduction produces species that are depleted in ^{34}S (or negative $\delta^{34}S$ values).

$\delta^{34}S$ (SO_4) values of water samples from the ÇG vary from 8.07‰ to 14.91‰ (VCDT) (average 13.25‰) and $\delta^{18}O$ (SO_4) values fall in the range of 11.73‰ to 12.23‰ (VSMOW) (Table 2). $\delta^{34}S$ of gypsum minerals from evaporitic units in the Sandak Unit varies between 15.0‰ and 18.1‰ (Gündoğan et al., 2008) which are quite consistent with those of studied waters. The source of sulfur in waters is reviewed on the $\delta^{18}O$ (SO_4) vs. $\delta^{34}S$ (SO_4) diagram (Figure 9). This diagram shows that sulfate in studied waters is derived from a Devonian-Lower Triassic source. Gündoğan et al. (2008) report that gypsum minerals within the Sandak Unit at the east of Honaz have $^{87}Sr/^{86}Sr$ ratios of 0.707761 to 0.707772 corresponding to Late Triassic period. It is clear that gypsum deposits of marine origin (10‰ to 35‰; Clark and Fritz, 1997) are the major sulfur contributor to the samples. $\delta^{34}S$ (SO_4) values and molar Ca^{2+}/SO_4^{2-} ratios of Ca-SO_4 type waters (nearly one) support the marine origin of sulfate. Gypsum and anhydrite minerals occur not only in large evaporite deposits but also form as minor sulfate nodules or laminae on the surface of limestone and dolomite layers (Clark and Fritz, 1997). In the study area, CAS might be the major source of Ca-HCO_3 type waters that have lower SO_4^{2-} concentration. Rotten-egg odor emitting from thermal waters is indicative of the presence of $H_2S(g)$ and sulfate reduction process.

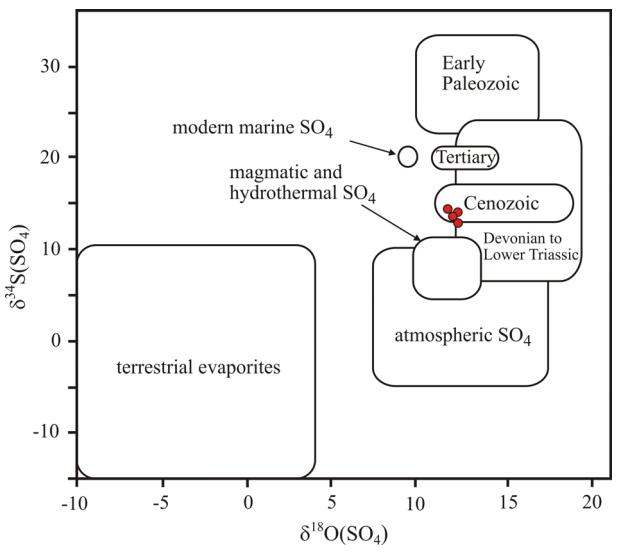

Figure 9. $\delta^{18}O$ (SO_4) vs. $\delta^{34}S$ (SO_4) diagram for the thermal waters.

5.3 Mineral saturation of waters

Studying the mineral saturation of natural waters is important for the awareness of scaling problems that could be come across during drilling and managing hot springs and in the production and transfer of thermal water from the wells. For this reason, it is necessary to determine the saturation states of minerals that are likely to form encrusting. In order to test the saturation tendency of waters, mineral saturations were calculated at discharge temperature of waters. PhreeqCi program (Parkhurst and Appelo, 1999) was used to estimate the saturation indices of carbonate, sulfate, and silica minerals. Positive values of saturation index indicate oversaturation while negative values stand for undersaturation, and computed indices at or close to zero (log SI = 0) point to equilibrium between the water and mineral. Except for Kazanpınar and Böceli springs (samples 7 and 14), carbonate minerals (calcite and dolomite) show over saturation behavior, as also revealed by the widespread distribution of travertine deposits in the ÇG (Figure 10a). Quartz is oversaturated whilst all the waters are undersaturated with respect to gypsum (Figure 10b).

There are four major processes responsible for travertine deposition (Pentecost, 2005): (1) Travertine precipitation from CO_2 that escapes from ascending deep Ca– and CO_2–rich fluids. The majority of travertines are formed by this mechanism, (2) Travertine formation by the reaction between atmospheric CO_2 and hyper-alkaline groundwater, (3) Travertine precipitation by the mixing between Ca–rich groundwater and alkaline surface waters (groundwater alkalization) and (4) Travertine formation by the common-ion effect.

In the study area, the release of dissolved CO_2 gas from the waters that are in contact with the atmosphere results in travertine crystallization (in calcite form) from the $CaCO_3$–saturated waters. The majority of Çürüksu waters precipitate $CaCO_3$ during their emergence at the surface or natural flow within the canal. Photographs of some springs and wells, and recent travertine and tufa formations are presented in Figures 11a–11e. Travertine terraces within the Kaklık cave are precipitated from the İçgöl spring (T = 23.4 °C, sample no 5). They resemble terrace-type Pamukkale travertines and are a good example for recent travertine formation in the area (Figure 11a). Some part of Pınarbaşı spring waters (sample 13) are discharged into a pool via a 1595 m-length canal along which pH value of waters increased from 7.16 to 7.98 (nearly one unit) and Ca^{2+} and CO_2 concentrations decreased from 106 to 84 mg/L and from 69 to 38 mg/L, respectively (Horvatincic et al., 2005). In a cascade at the end of this canal $CaCO_3$ (tufa) is precipitated (Figure 11e).

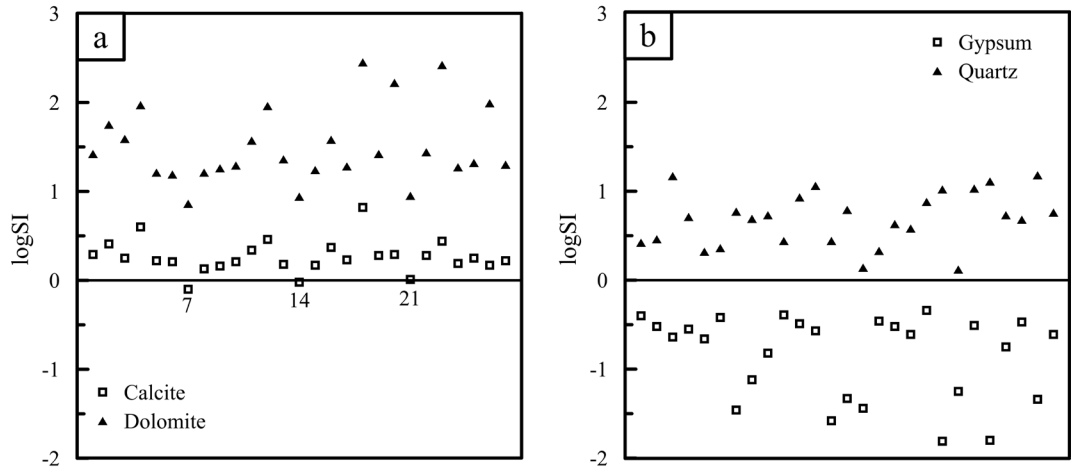

Figure 10. Saturation of waters with respect to (a) calcite and dolomite and (b) gypsum and quartz.

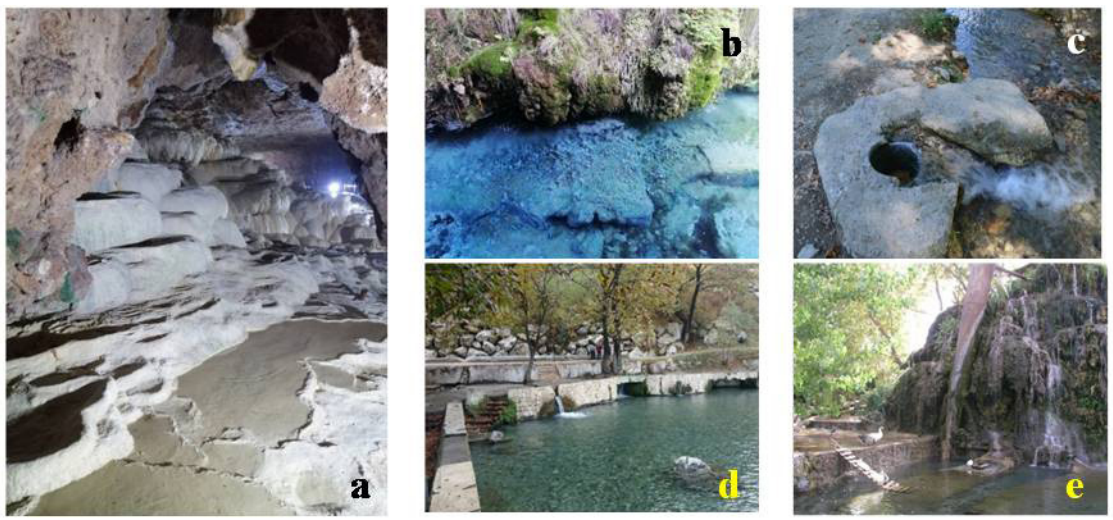

Figure 11. (a) Recent travertine precipitation in the Kaklık cave, (b) İçgöl spring within the cave (23.4 °C), (c) Well 7 (24.6 °C), (d) Pınarbaşı spring (19.6 °C), it is discharged into a pool and from there it is delivered to the irrigation system via canals, (e) Recent tufa formation on the cascade of the Pınarbaşı spring.

The common-ion effect is another process responsible for travertine deposition. Ca-HCO_3 type waters discharging from the carbonate rocks of the Menderes Massif are mixed with Ca-SO_4 type waters issuing from the Sandak Unit and, as a result, Ca^{2+} content of water is increased. This gave rise to an increase in calcite saturation of water facilitating calcite (travertine) deposition:

$$Ca^{2+} + HCO_3^- + CaSO_4.2H_2O \rightarrow Ca^{2+} + SO_4^{2-} + CaCO_3 \downarrow + H^+ + 2H_2O \quad (5)$$

By the calcite precipitation SO_4^{-2} concentration in waters relatively increases and Ca^{+2}/SO_4^{-2} ratio decreases (Figure 12). Gypsum dissolution decreases the solubility of both limestone and dolomite (increase in Ca^{2+} and SO_4^{2-} in waters).

XRD analysis of travertine and tufa samples collected from the field indicated that calcite and slight amount of aragonite and quartz are the major mineral phases (Özkul et al., 2013) which is consistent with the results of saturation calculations. In the light of above findings, it is concluded that unless necessary precautions are taken, carbonate scaling will be a serious problem in Çürüksu when the thermal waters are utilized for any type of industrial or balneological purpose.

Sr isotope composition of travertines is generally derived from the carbonate source rocks (Minissale et al., 2002). $^{87}Sr/^{86}Sr$ ratios of Ballık travertines (Ece and Faber

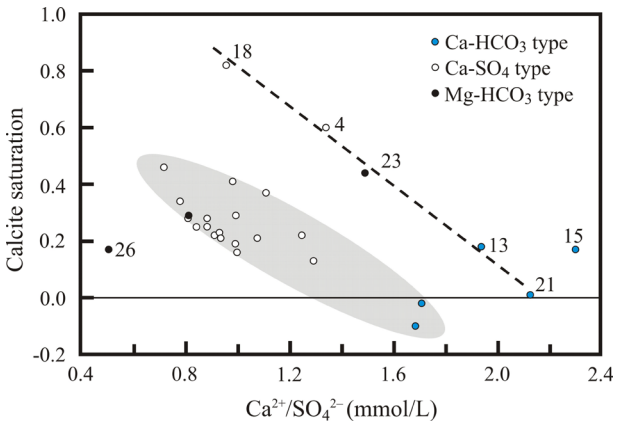

Figure 12. Calcite saturation vs. Ca^{2+}/SO_4^{2-} graphic for the waters.

quarries) at 3 km NW of the İçgöl spring (sample no 5) are reported 0.70785 to 0.70792 (Claes et al., 2015). In another work on travertines from the Çakmak quarry, El Desouky et al. (2015) found similar $^{87}Sr/^{86}Sr$ ratios and suggested that Triassic limestones of the Lycian nappes are the source rock of Sr in travertines. This conclusion is consistent with our findings from the water chemistry studies.

5.4. Geothermometry applications

Geothermometers are used to estimate the temperature of geothermal fluid within the reservoir. In order to determine the sort of geothermal fluid use (e.g., electricity production, house heating and greenhouse), reservoir temperature needs to be estimated before the exploitation. For this, several solute, gas and isotope geothermometer methods were developed particularly over the 50–60 years. In this study, for the calculation of reservoir temperature of Çürüksu thermal waters, Li, chalcedony, quartz, Ca/Mg, anhydrite-chalcedony (quartz) chemical geothermometers and sulfate-water isotope geothermometer were used. The results of calculations are shown in Table 4.

5.4.1. Chemical geothermometers

Chemical geothermometers consist of silica geothermometers that are based on temperature-dependent solubility of various silica phases (e.g., Fournier, 1977; Arnorsson et al., 1983) and the cation geothermometers that are based on ion exchange reactions with temperature-dependent equilibrium constants (Na-K: Truesdell, 1976; Arnorsson et al., 1983; Giggenbach, 1988; Na-K-Ca: Fournier and Truesdell, 1973; Fournier and Potter, 1979; Na-Li: Fouillac and Michard, 1981; K-Mg: Giggenbach, 1988; Li-Mg: Kharaka and Mariner, 1989).

Among the cation geothermometers applied to studied waters, very high temperatures were computed by the Na-K and Li-Mg geothermometers (191–309 °C and 367–527 °C, respectively) whereas those estimated by Na-Li geothermometer (Fouillac and Michard, 1981; Cl < 0.3 M) are moderately high (89–149 °C). The K-Mg geothermometer gave reservoir temperatures close to the discharge temperatures but the Na-K-Ca geothermometer yielded lower values than the outlet temperatures. Results of Li geothermometer (Fouillac and Michard, 1981) are likely to be realistic (41–87 °C), however, low Li concentrations in samples (max. 0.102 mg/L) make such temperature values ambiguous.

Giggenbach (1988) proposed $Na/1000\text{-}K/100\text{-}Mg^{1/2}$ triangular diagram to estimate the reservoir temperatures of waters equilibrated with the reservoir rock and suggested that geothermal waters plotting into the "immature waters field" are not suitable for the application of cation geothermometers. In this diagram, Mg% is found from the relation of (where units in mg/L):

$$Mg\% = 100 \cdot Mg^{1/2} / S$$
$$S = (Na/1000) + (K/100) + Mg^{1/2}$$

Na^+ and K^+ concentrations of the Çürüksu thermal waters are low (Na^+: 9.4–39.7 mg/L, K^+: 1.23–4.36 mg/L) but Mg^{2+} contents are very high (40–131 mg/L). Mg% computed by the above equation is from 99.1% to 99.7%, and therefore, in the Na-K-Mg diagram all the waters might plot very close to the Mg apex. For this reason, Çürüksu waters are immature waters and reservoir temperatures estimated from the cation geothermometers are not discussed further because they are considered unrealistic.

Silica geothermometers are based on temperature-dependent ion exchange reactions between thermal waters and various silica phases in the reservoir. Reservoir temperature and quartz-controlled silica concentration are well correlated at temperatures above 180 °C (Arnorsson, 1975). At lower temperatures (<110 °C), silica concentration is mostly controlled by chalcedony and even cristobalite or amorphous silica at much lower temperatures. Quartz slowly precipitates at lower temperatures (i.e. <100 °C) and hence, saturation is rarely achieved (Rimstidt and Barnes, 1980). However, quartz geothermometer might yield consistent results even at low or moderate temperatures (Blasco et al., 2018).

The chalcedony geothermometer applied to Çürüksu thermal waters yielded reservoir temperatures of 38–52 °C (except for Ca-HCO_3 type wells 1 and 7). Among the thermal waters only the wells 1 and 7 are not saturated with respect to chalcedony (SI: –0.13 and –0.16) and chalcedony geothermometer for these waters gave reservoir temperatures close to or lower than the measured temperatures. Quartz geothermometer values of these two samples are 49 and 59 °C, which are consistent with chalcedony temperatures of other thermal waters. Reservoir temperatures estimated by the quartz geothermometer fall in the range of 49 to 83 °C and are about 30 °C greater than the chalcedony temperatures. Silica geothermometers are

greatly affected by some physical processes such as boiling and dilution. Since Çürüksu waters might be produced by the mixing between thermal fluid and cold groundwater, SiO_2 content of thermal waters may be different from the reservoir. However, no spring or well water is available as the end member of geothermal fluid to apply the silica-enthalpy model and estimate the mixing ratio.

According to Chiodini et al. (1995), Ca^{2+}, Mg^{2+}, and SO_4^{2-} concentrations and $SO_4^{2-}/(F^-)^2$ and Ca^{2+}/Mg^{2+} ratios of geothermal fluids within low-moderate temperature hydrothermal systems consisting of carbonate-evaporite units could be used as potential geothermometers. Chiodini et al. (1995) also suggested that $(HCO_3^-)^2/SO_4^{2-}$ ratio is indicative of P_{CO2} and $(HCO_3^-)/F^-$ ratio and HCO_3^- concentration stand for both temperature and P_{CO2}. The same authors stated that these geoindicators could be used to estimate reservoir temperature of hydrothermal systems made up of carbonate-evaporite rocks with temperatures of 50–150 °C. For this, they proposed a HCO_3-SO_4-F ternary diagram with theoretical T–Pco_2 grids (Figure 13). In this diagram, samples 15 and 21 of Ca-HCO_3 type plot close to 90 °C interval and indicate high P_{CO2} whereas Ca-SO_4 type waters plot at pressure values of 1–10 bar and temperatures of 50–75 °C. The majority of waters are clustered around 70–80 °C.

Ca/Mg and SO_4-F geothermometers (Chiodini et al., 1995) developed for carbonate-evaporite systems were applied to the Çürüksu samples. Since anhydrite-fluorite and gypsum-fluorite equilibriums are not established in the studied waters, SO_4-F geothermometer yielded negative temperatures and thus, results of this geothermometer are not reliable. Ca-Mg geothermometer gave temperatures of 73 to 96 °C, which are slightly higher than those computed by the quartz geothermometer (49–83 °C). Due to uncertainties related to the crystallinity and solubility of dolomite, it may not be possible to obtain a reliable result for reservoir temperature (Blasco et al., 2019).

Pastorelli et al. (1999) state that Mesozoic carbonate-evaporite units are the reservoir rocks of Ca-SO_4 type warm springs and Ca-SO_4-HCO_3 type mineral waters in the Acquarossa geothermal field, Switzerland. They suggested that chalcedony and anhydrite are equilibrated at similar temperatures and concluded that this mineral pair reflects the most accurate reservoir temperature within a narrow array. This method was applied to thermal waters in Bagnères-de-Bigorre (France) (Levet et al., 2002), Xinzhou and Shenzao in China (Wang et al., 2018), Yenicekent and Gölemezli in Turkey (Alçiçek et al., 2016, 2018) and Tiermas and Arnedillo in Spain (Blasco et al., 2017, 2018) and realistic reservoir temperatures were obtained.

Anhydrite-chalcedony and anhydrite-quartz saturation diagrams constructed for Çürüksu samples at a temperature of range of 20–100 °C are shown in Figures 14a and 14b. In these graphics, anhydrite and chalcedony saturation

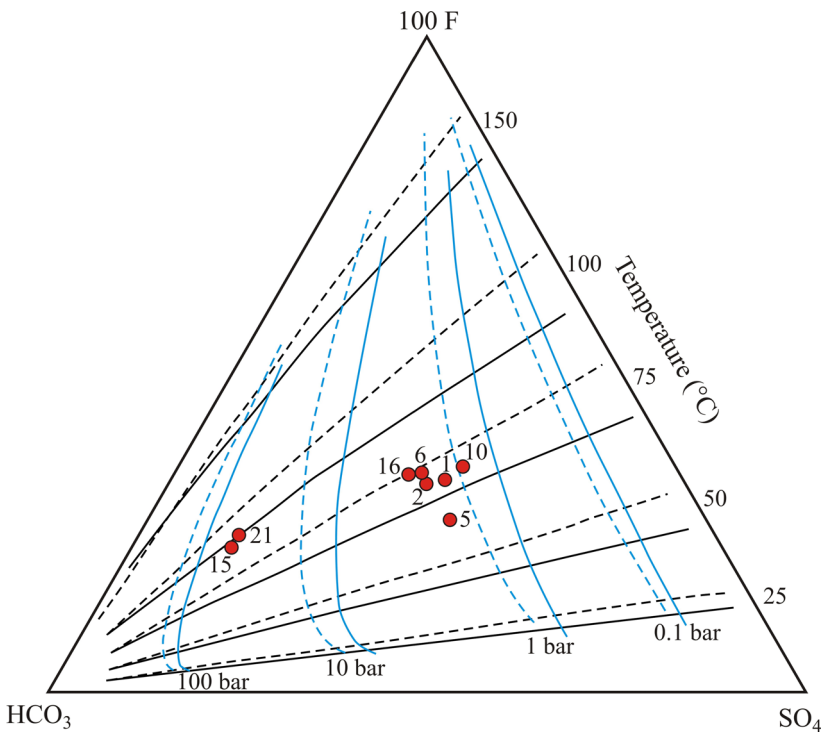

Figure 13. HCO_3-SO_4-F ternary diagram (Chiodini et al., 1995). Theoretical T-Pco_2 grids show Cl contents of 0.001 mol/kg (dotted line) and 0.1 mol/kg (solid line).

curves intersect the equilibrium line (logQ/K=0) at around 63–75 °C and anhydrite and quartz curves are equilibrated at temperatures of 74–86 °C. These results are consistent with temperature estimations by quartz and Ca-Mg geothermometer.

5.4.2 Sulfate-water isotopic geothermometer

Sulfate-water isotope geothermometer is based on oxygen isotope exchange between SO_4 and H_2O as a function of temperature (Lloyd, 1968; Mizutani and Rafter 1969; Mizutani, 1972). This geothermometer has been successfully applied to several water-dominated geothermal systems at temperatures of 100–350 °C (Mizutani and Rafter 1969; Mizutani 1972; Cortecci 1974; Cortecci and Dowgiallo 1975; McKenzie and Truesdell 1977; Fouillac et al., 1990).

Experimental studies showed that pH of a near-neutral-pH chloride reservoir fluid did not significantly affect the state of equilibrium fractionation provided that residence times exceed the equilibration periods of 18 years for a 200 °C–fluid or 2 years for a 300 °C–fluid (Nicholson, 1993). The longer residence times of the geothermal water would then be a critical factor for the establishment of isotopic equilibrium as slow reequilibration periods ensure that no isotopic exchange will occur during fluid ascend to the surface. The isotopic composition of the surface waters and the temperatures estimated from the geothermometers, are therefore likely to reveal the equilibrium conditions in the reservoir (Nicholson, 1993). However, due to several physicochemical processes including boiling, dilution, mixing and atmospheric oxidation of hydrogen sulfide, deep reservoir fluid and its surface discharge may not always have the same isotopic composition, which might alter the temperature estimate by H_2O–SO_4 geothermometer. Low reservoir temperatures necessitate long residence time to attain isotopic equilibrium (e.g., 500 years at l00 °C) and this makes geothermometer estimations inapplicable to low-temperature systems unless residence times are extremely prolonged (Nicholson, 1993). Radiocarbon (^{14}C) dating analysis for three springs in the study area yielded 4091 (İçgöl spring, sample 5 in Table 1), 5945 and 9631 years (Önhon et al., 1989). This might indicate that Çürüksu waters have sufficient time for isotopic equilibration.

According to Boschetti (2013), application of $^{18}O(SO_4$-$H_2O)$ geothermometer to the low-enthalpy fields is very useful to confirm the results of chemical geothermometers. $\delta^{18}O(SO_4$-$H_2O)$ geothermometer applied to the Tiermas (Blasco et al., 2017) and Arnedillo (Blasco et al., 2018) thermal waters yielded reservoir temperatures significantly less than the discharge temperatures. This is attributed to the fact that ^{18}O exchange between SO_4^{2-} and H_2O occurred very slowly due to low reservoir temperature that eventually prevented the equilibration.

Reservoir temperatures computed for the Çürüksu thermal waters (İçgöl, Kokarsu, Halkabaşı and well 7) using the $\delta^{18}O(SO_4$-$H_2O)$ geothermometer equations proposed by Lloyd (1968) and Mizutani and Rafter (1969) fall in the range of 65 to 81 °C. These temperatures seem to be consistent with those estimated by the quartz, Li, Ca-Mg and anhydrite-chalcedony (quartz) geothermometers. Equations of Halas and Pluta (2000) and Zeebe (2010) yielded temperature ranges of 27–31 °C (2 to 9 °C greater than the discharge temperatures) and 33–38 °C. These temperatures are slightly lower than the chalcedony geothermometer results and thus considered not accurate. In conclusion, temperatures of 65–81 °C from the

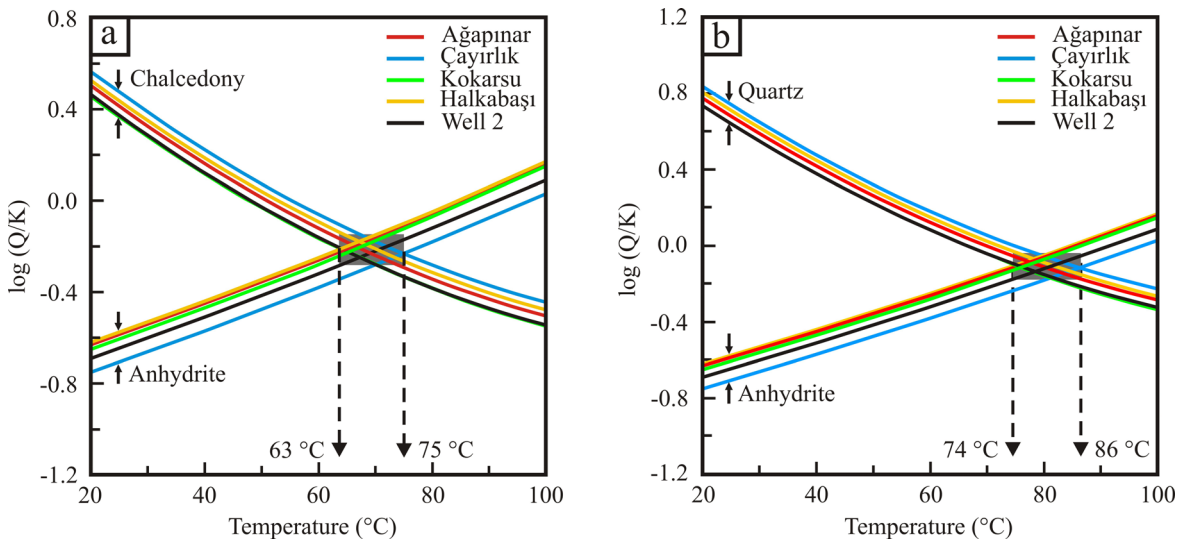

Figure 14. Saturation diagrams constructed for a temperature of range of 20–100 °C; (a) anhydrite-chalcedony and (b) anhydrite-quartz.

$\delta^{18}O(SO_4\text{-}H_2O)$ geothermometer, 75 °C from the HCO_3-SO_4-F diagram, 65–76 °C from the anhydrite-chalcedony diagram and 45–80 °C estimated by the chalcedony and quartz geothermometers are mostly consistent. Then, a reservoir temperature range of 60 ± 15 °C is suitable for the Çürüksu thermal waters.

5.4.3. Estimation of paleotemperatures of travertine-forming fluids

Oxygen isotope exchange between calcite and water provides a good opportunity to estimate the temperature of travertine-forming fluids. Özkul et al. (2013) studied deposition and geochemical characteristics of several Quaternary travertine deposits in the Denizli basin. For the calculation of paleofluids temperature, they used $\delta^{18}O_{water}$ of recent springs that are manifested close to the travertine deposits and it was assumed that the oxygen isotope values of the paleosprings were similar to those of the modern springs. Paleofluid temperatures estimated by the oxygen isotope fractionation yielded temperatures of 22–26 °C for Kelkaya, 22–30 °C for Honaz, 23–39 °C for Ballık and 47–56 °C for the Kocabaş travertines (Özkul et al., 2013; Claes et al., 2015). These temperatures are consistent with the results of chalcedony and isotope geothermometers of Halas and Pluta (2000) and Zeebe (2010) but about 20 °C lower than estimates of other chemical and isotope geothermometers.

Homogenization temperatures measured on primary fluid inclusions (FI) of Pamukkale travertines yielded 132–145 °C (Rizzo et al., 2019). These temperatures are notably higher than those estimated by chemical and isotopic geothermometers and discharge temperatures of waters that recently precipitate travertines. Salinities of FIs from the same travertines fall in the range of 0.4 to 7.0 wt% NaCl equivalent (Rizzo et al., 2019), which are too low to suggest a long residence time for interaction with the source rocks. Our findings agree with the results of Uysal et al. (2007) who suggested that Pamukkale fissure travertine did not precipitate from high- temperature fluids. As a final note, the absence of any $\delta^{18}O$ shift in waters indicates that reservoir temperature is less than 100 °C.

6. Conclusion

The eastern termination of the Büyük Menderes Graben in western Turkey hosts several low-temperature springs. These waters with neutral pH values and temperatures of 20 to 25 °C are manifested through a carbonate reservoir in the ÇG. Thermal waters are represented by Ca-HCO_3 and Ca-SO_4 types and cold waters are dominated by Ca-HCO_3, Ca-SO_4 and Mg-HCO_3.

Oxygen and hydrogen isotope values of the Çürüksu waters point to a meteoric origin with local recharge. Using the altitude vs. $\delta^{18}O$–δD equations proposed for the Pamukkale geothermal field, recharge elevations for the studied waters are found in the range of 685 to 2163 m. Tritium concentrations of thermal waters (0.12 to 2.17 TU) are lower than cold waters (0.28 to 6.08 TU) and indicate relatively longer residence time for hot waters. Carbon isotope compositions of samples varying over a wide range from –9.52‰ to +2.88‰ have multiple sources of carbon. Carbon in thermal waters is likely to originate from metamorphic CO_2 or the dissolution of marine carbonates whereas carbon in cold waters is derived from an organic source. $\delta^{34}S$ and $\delta^{18}O$ of dissolved sulfate in the samples waters show that sulfur is derived from dissolution of marine gypsum deposits.

Çürüksu waters are likely to be equilibrated with calcite, dolomite and quartz but undersaturated with respect to gypsum. Chemical and isotopic evaluations imply that the variations in the water chemistry of samples is due to a combination of processes including water-rock interaction, ion exchange and mixing of various types of waters. Since Çürüksu waters are of immature character, reservoir temperatures were estimated with the use of several silica and unconventional geothermometers. Temperatures calculated by the chalcedony, quartz and Ca-Mg geothermometers are 21–52 °C, 49–83 °C and 73–96 °C. HCO_3-SO_4-F and anhydrite-chalcedony (quartz) diagrams gave a temperature range of 63–86 °C and $^{18}O(SO_4\text{-}H_2O)$ isotope geothermometer estimated 67–78 °C.

Considering heat flow and geothermal gradient values, the ÇG is a promising target for geothermal energy exploration. Therefore, results of this study are expected to constitute a basis for future geothermal surveys. Results of chemical and isotopic geothermometers indicate reservoir temperature of 60 ± 15 °C that requires drilling to a depth of at least 1000 m for the production of thermal water. Water extracted may be used for balneotherapy and greenhouse heating.

7. Acknowledgement

This study was financially supported by the Scientific Research Coordination Unit of Pamukkale University (grant number 2015FBE049). The authors are grateful to two anonymous referees and Özgür Avşar for their critical comments that improved the manuscript.

References

Akkuş İ, Akıllı H, Ceyhan S, Dilemre A, Tekin Z (2005). Türkiye jeotermal kaynaklar envanteri. Maden Tetkik ve Arama Genel Müdürlüğü Envanter Serisi: 201 (in Turkish).

Alçiçek H, Bülbül A, Alçiçek MC (2016). Hydrogeochemistry of the thermal waters from the Yenice Geothermal Field (Denizli Basin, Southwestern Anatolia, Turkey). Journal of Volcanology and Geothermal Researches 309: 118–138. doi: 10.1016/j.jvolgeores.2015.10.025

Alçiçek H, Bülbül A, Brogi A, Liotta D, Ruggieri G et al. (2018). Origin, evolution and geothermometry of the thermal waters in the Gölemezli Geothermal Field, Denizli Basin (SW Anatolia, Turkey). Journal of Volcanology and Geothermal Researches 349: 1–30. doi: 10.1016/j.jvolgeores.2017.07.021

Alçiçek H, Bülbül A, Yavuzer İ, Alçiçek MC (2019a). Hydrogeochemical and isotopic assessment and geothermometry applications in relation to the Karahayıt Geothermal Field (Denizli Basin, SW Anatolia, Turkey). Hydrogeology Journal. doi: 10.1007/s10040-019-01927-y

Alçiçek H, Bülbül A, Yavuzer İ, Alçiçek MC (2019b). Origin and evolution of the thermal waters from the Pamukkale Geothermal Field (Denizli Basin, SW Anatolia, Turkey): Insights from hydrogeochemistry and geothermometry. Journal of Volcanology and Geothermal Research **372:** 48–70. doi: 10.1016/j.jvolgeores.2018.09.011

Arnorsson S (1975). Application of the silica geothermometer in low temperature hydrothermal areas in Iceland. American Journal of Science 275: 763–784. doi: 10.2475/ajs.275.7.763

Arnorsson S, Gunnlaugsson E, Svavarsson H (1983). The chemistry of geothermal waters in Iceland. III. Chemical geothermometry in geothermal investigations. Geochimica et Cosmochimica Acta 47 (3): 567–577. doi: 10.1016/0016-7037(83)90278-8

Avşar Ö, Altuntaş G (2017). Hydrogeochemical evaluation of Umut geothermal field (SW Turkey). Environmental Earth Sciences 76: 582. doi: 10.1007/s12665-017-6929-6

Baba A, Sözbilir H (2012). Source of arsenic based on geological and hydrogeochemical properties of geothermal systems in western Turkey. Chemical Geology 334: 364–377. doi: 10.1016/j.chemgeo.2012.06.006

Bilim F, Akay T, Aydemir A, Koşaroğlu S (2016). Curie point depth, heat-flow and radiogenic heat production deduced from the spectral analysis of the aeromagnetic data for geothermal investigation on the Menderes Massif and the Aegean Region, western Turkey. Geothermics 60: 44–57**.** doi: 10.1016/j.geothermics.2015.12.002

Blasco M, Auqué LF, Gimeno MJ, Acero P, Asta MP (2017). Geochemistry, geothermometry and influence of the concentration of mobile elements in the chemical characters of carbonate-evaporitic thermal systems. The case of the Tiermas geothermal system (Spain). Chemical Geology 466: 696–709. doi: 10.1016/j.chemgeo.2017.07.013

Blasco M, Gimeno MJ, Auqué LF (2018). Low temperature geothermal systems in carbonate-evaporitic rocks: mineral equilibria assumptions and geothermometrical calculations. Insights from the Arnedillo thermal waters (Spain). The Science of the Total Environment 615: 526–539. doi: 10.1016/j.scitotenv.2017.09.269

Blasco M, Auquéa LF, Gimenoa MJ, Aceroa P, Gómeza J et al. (2019). Mineral equilibria and thermodynamic uncertainties in the geothermometrical characterisation of carbonate geothermal systems of low temperature. The case of the Alhama-Jaraba system (Spain). Geothermics 78: 170–182. doi: 10.1016/j.geothermics.2018.11.004

Bogomolov GV, Silin-Bekcurin AI (editors) (1955). Special Hydrogeology. Moscow, Soviet Union: Gosgeoltekhizdat (in Russian).

Boschetti T (2013). Oxygen isotope equilibrium in sulfate-water systems: a revision of geothermometric applications in low-enthalpy systems. Journal of Geochemical Exploration 124: 92–100. doi: 10.1016/j.gexplo.2012.08.011

Bozkurt E (2001). Neotectonics of Turkey – a synthesis. Geodinamica Acta 14: 3–30. doi: 10.1080/09853111.2001.11432432

Bozkuş C, Kumsar H, Özkul M, Hançer M (2001). Seismicity of active Honaz Fault under an extentional tectonic regime. In: International Earth Science Colloquium on the Aegean Region; İzmir, Turkey. pp. 7–16.

Cermak V, Hurtig E (1979). Heat flow map of Europe, 1/5,000,000. In: Cermak V, Rybach L (editors). Terrestrial heat flow in Europe. Springer-Verlag, Berlin Heidelberg, Germany. pp. 3-40.

Chiodini G, Frondini F, Marini L (1995). Theoretical geothermometers and PCO_2 indicators for aqueous solutions coming from hydrothermal systems of medium–low temperature hosted in carbonate-evaporite rocks. Application to the thermal springs of the Etruscan Swell. Italy. Applied Geochemistry 10 (3): 337–346. doi: 10.1016/0883-2927(95)00006-6

Claes H, Török A, Soete J, Mohammadi Z, Vassilieva E et al. (2020). U/Th dating and open system behavior: implications for travertines based on the study of Süttő (Hungary) and Ballik (Turkey) sites. Quaternaire 31 (2): 117-132. doi: 10.4000/quaternaire.13728

Claes H, Soete J, VanNoten K, El Desouky H, Erthal MM et al. (2015). Sedimentology, three–dimensional geobody reconstruction and carbondioxide origin of Pleistocene travertine deposits in the Ballık area (south-west Turkey). Sedimentology 62: 1408–1445. doi: 10.1111/sed.12188

Clark ID, Fritz P (editors) (1997). Environmental Isotopes in Hydrogeology. New York, USA: Lewis Publishers.

Craig H (1961). Isotopic variations in meteoric waters. Science 133: 1702–1703. doi: 10.1126/science.133.3465.1702

Cortecci G (1974). Oxygen isotopic ratios of sulfate ions-water pairs as a possible geothermometer. Geothermics 3: 60–64. doi: 10.1016/0375-6505(74)90021-2

Cortecci G, Dowgiałło J (1975). Oxygen and sulfur isotopic composition of the sulfate ions from mineral and thermal groundwaters of Poland. Journal of Hydrology 24: 271–282. doi:10.1016/0022-1694(75)90085-2

Crossey LJ, Fischer TP, Patchett JP, Karlstrom KE, Hilton DR et al. (2006). Dissected hydrologic system at the Grand Canyon: interaction between deeply derived fluids and plateau aquifer waters in modern springs and travertine. Geology 34: 25–28. doi: 10.1130/G22057.1

Dilaver AT, Aydın B, Özyurt NN, Bayarı CS (2018). Türkiye Yağışlarının İzotop İçerikleri (2012-2016). Devlet Su İşleri Genel Müdürlüğü-Teknik Araştırma ve Kalite Kontrol Dairesi Başkanlığı ve Meteoroloji Genel Müdürlüğü-Araştırma Dairesi Başkanlığı, Ankara, Türkiye (in Turkish).

El Desouky H, Soete J, Claes H, Özkul M, Vanhaecke F et al. (2015). Novel applications of fluid inclusions and isotope geochemistry in unraveling the genesis of fossil travertine systems. Sedimentology 62 (1): 27–56. doi: 10.1111/sed.12137

Emre Ö, Duman TY, Özalp S, Elmacı H (2011). 1:250.000 scale active fault map series of Turkey, Denizli (NJ 35-12) Quadrangle. Serial number: 12, General Directorate of Mineral Research and Exploration, Ankara, Turkey.

EPDK (Energy Market Regulatory Authority of Turkey) (2021). Electricity Market Development Report 2021, Ankara [online]. Website www.epdk.gov.tr/Detay/Icerik/1-1271/electricityreports [accessed 25 November 2021].

Evans EA (1966). Tritium and its Compounds. Princeton, N.J,. Van Nostrand, 441p.

Fouillac C, Fouillac AM, Criaud A (1990). Sulphur and oxygen isotopes of dissolved sulphur species in formation waters from the Dogger geothermal aquifer, Paris Basin, France. Applied Geochemistry 5 (4): 415–427. doi: 10.1016/0883-2927(90)90018-Z

Fouillac C, Michard G (1981). Sodium/Lithium ratio in water applied to geothermometry of geothermal reservoirs. Geothermics 10 (1): 55–70. doi: 10.1016/0375-6505(81)90025-0

Fournier RO (1977). Chemical geothermometers and mixing models for geothermal systems. Geothermics 5: 41–50. doi: 10.1016/0375-6505(77)90007-4

Fournier RO, Truesdell AH (1973). An empirical Na-K-Ca geothermometer for natural waters. Geochimica et Cosmochimica Acta 37 (5): 1255–1275. doi: 10.1016/0016-7037(73)90060-4

Fournier RO, Potter RW (1979). Magnesium correction to the Na-K-Ca chemical geothermometer. Geochimica et Cosmochimica Acta 43 (9): 1543–1550. doi: 10.1016/0016-7037(79)90147-9

Gat JR, Carmi I (1970). Evolution of the isotopic composition of atmospheric waters in the Mediterranean Sea area. Journal of Geophysical Research 75 (15): 3039–3048. doi: 10.1029/JC075i015p03039

Giggenbach WF (1988). Geothermal solute equilibria - derivation of Na-K-Mg-Ca geoindicators. Geochimica et Cosmochimica Acta 52: 2749–2765. doi: 10.1016/0016-7037(88)90143-3

Güleç N, Hilton DR, Mutlu H (2002). Helium isotope variations in Turkey: relationship to tectonics, volcanism and recent seismic activities. Chemical Geology 187: 129–142. doi: 10.1016/s0009-2541(02)00015-3

Gündoğan İ, Helvacı C, Sözbilir H (2008). Gypsiferous carbonates at Honaz Dağı (Denizli): First documentation of Triassic gypsum in western Turkey and its tectonic significance. Journal of Asian Earth Sciences 32: 49–65. doi: 10.1016/j.jseaes.2007.09.005

Halas S, Pluta I (2000). Empirical calibration of isotope thermometer $\delta^{18}O$ (SO_4^{2-})–$\delta^{18}O$ (H_2O) for low temperature brines. In: V Isotope Workshop; Kraków, Poland. pp. 68–71.

Horvatinčić N, Özkul M, Gökgöz A, Barešić J (2005). Isotopic and geochemical investigation of tufa in Denizli province, Turkey. In: 1st International Symposium on Travertine; Denizli, Turkey. pp. 162–170.

İlkışık OM (1995). Regional heat flow in western Anatolia using silica temperature estimates from thermal springs. Tectonophysics 244 (1-3): 175–184. doi: 10.1016/0040-1951(94)00226-Y

Izbicki JA, Christensen AH, Newhouse MW, Aiken GR (2005). Inorganic, isotopic, and organic composition of high–chloride water from wells in a coastal southern California aquifer. Applied. Geochemistry 20: 1496–1517. doi: 10.1016/j.apgeochem.2005.04.010

Kampschulte A, Strauss H (2004). The sulfur isotopic evolution of Phanerozoic seawater based on the analysis of structurally substituted sulfate in carbonates. Chemical Geology 204: 255–286. doi: 10.1016/j.chemgeo.2003.11.013

Karakuş H, Şimşek Ş (2013). Tracing deep thermal water circulation systems in the E–W trending Büyük Menderes Graben, western Turkey. Volcanology and Geothermal Researches 252: 38–52. doi: 10.1016/j.jvolgeores.2012.11.006

Kaya A (2015). The effects of extensional structures on the heat transport mechanism: An example from the Ortakçı geothermal field (Büyük Menderes Graben, SW Turkey). Journal of African Earth Sciences 108: 74–88. doi: 10.1016/j.jafrearsci.2015.05.002

Kele S, Özkul M, Forizs I, Gökgöz A., Baykara MO et al. (2011). Stable isotope geochemical and facies study of Pamukkale travertines: new evidences of low temperature non-equilibrium calcite-water fractionation. Sedimentary Geology 238: 191–212. doi: 10.1016/j.sedgeo.2011.04.015

Kendall C, Sklash MG, Bullen TD (1995) Isotope tracers of water and solute sources in catchments. In: Trudgill ST (editor). Solute modeling in catchment systems. New York, USA: John Wiley and Sons, pp. 261–303.

Kharaka YK, Mariner RH (1989). Chemical geothermometers and their application to formation waters from sedimentary basins. In: Naeser ND, McCulloh T (Editors). Thermal History of Sedimentary Basins: Methods and Case Histories. New York, USA: Springer–Verlag, pp. 99–117.

Koçyiğit A (2005). Denizli Graben-Horst System and the eastern limit of the west Anatolian continental extension: Basin fill, structure, deformational mode, throw amount and episodic evolutionary history, SW Turkey. Geodinamica Acta 18: 167–208. doi: 10.3166/ga.18.167-208.

KOERI (Kandilli Rasathanesi ve Deprem Araştırma Enstitüsü) (2021). Recent Earthquakes in Turkey [online].

Website http://www.koeri.boun.edu.tr/sismo/zeqdb/default.asp [accessed 08 April 2021].

Konak N, Şenel M (2002). Geological map of Turkey in 1:500000 scale: Denizli sheet. General Directorate of Mineral Research and Exploration of Turkey.

Krouse HR (1976). Sulphur isotope variations in thermal and mineral waters. In: International Symposium on Water-Rock Interaction; Prague, Czechoslovakia. pp. 340–347.

Krouse HR, Mayer B (2000). Sulphur and oxygen isotopes in sulphate. In: Cook P, Herczeg AL (editors). Environmental tracers in subsurface hydrology. Norwell, MA, USA: Kluwer Academic Publishers, pp. 195–231. doi: 10.1007/978-1-4615-4557-6_7

Levet S, Toutain JP, Munoz M, Berger G, Negrel P et al. (2002). Geochemistry of the Bagnéres-de-Bigorre thermal waters from the North Pyrenean Zone (France). Geofluids 2: 25–40. doi: 10.1046/j.1468-8123.2002.00030.x

Lloyd RM (1968). Oxygen isotope behaviour in the sulfate-water system. Journal of Geophysical Research 73: 6099–6110. doi:10.1029/JB073i018p06099

Lucas LL, Unterweger MP (2000). Comprehensive review and critical evaluation of the half-life of tritium. Journal of Research of the National Institute of Standards and Technology 105 (4): 541-549.

Mayo AL, Loucks MD (1995). Solute and isotopic geochemistry and ground water flow in the central Wasatch Range, Utah. Journal of Hydrology 172 (1-4): 31–59. doi: 10.1016/0022-1694(95)02748-E

McKenzie DP (1978). Active tectonics of the Alpine-Himalayan belt: the Aegean Sea and surrounding regions. Geophysical Journal International 55 (1): 217–254. doi: 10.1111/j.1365-246X.1978.tb04759.x

McKenzie WF, Truesdell AH (1977). Geothermal reservoir temperatures estimated from the oxygen isotope compositions of dissolved sulfate and water from hot springs and shallow drillholes. Geothermics 5: 51–61. doi: 10.1016/0375-6505(77)90008-6

McLean W, Jankowski J, Lavitt N (2000). Groundwater quality and sustainability in an alluvial aquifer, Australia. In: Sililo O et al. (editors). Groundwater, Past Achievements and Future Challenges. Rotterdam, The Netherlands: A.A. Balkema, pp. 567–573.

Meybeck M (1987). Global chemical weathering of surficial rocks estimated from river dissolved loads. American Journal of Science 287 (5): 401–428. doi: 10.2475/ajs.287.5.401

Minissale A, Kerrick DM, Magro G, Murrell MT, Paladini M et al. (2002). Geochemistry of Quaternary travertines in the region North of Rome (Italy): structural, hydrologic and paleoclimatologic implications. Earth and Planetary Science Letters 203: 709–728. doi: 10.1016/S0012-821X(02)00875-0

Mizutani Y (1972). Isotopic composition and underground temperature of the Otake geothermal water, Kyushu, Japan. Geochemical Journal 6: 67–73. doi: 10.2343/geochemj.6.67

Mizutani Y, Rafter TA (1969). Oxygen isotopic composition of sulphates. 3. Oxygen isotopic fractionation in the bisulfate ion-water system. New Zealand Journal of Science 12: 54–59.

Mutlu H, Güleç N (1998). Hydrogeochemical outline of thermal waters and geothermometry applications in Anatolia, Turkey. Journal of Volcanology and Geothermal Research 85: 495–515. doi: 10.1016/S0377-0273(98)00068-7

Mutlu H, Güleç N, Hilton DR, Aydın H, Halldorsson SA (2012). Spatial variations in gas and stable isotope compositions of thermal fluids around Lake Van: implications for crust–mantle dynamics in eastern Turkey. Chemical Geology 300–301: 165-176. doi: 10.1016/j.chemgeo.2012.01.026

Mutlu H, Güleç N, Hilton DR (2008). Helium-carbon relationships in geothermal fluids of western Anatolia, Turkey. Chemical Geology 247: 305–321. doi: 10.1016/j.chemgeo.2007.10.021

Nicholson K (editor) (1993). Geothermal Fluids: Chemistry and Exploration Techniques. Berlin, Heidelberg, Germany: Springer–Verlag.

Okay Aİ (1989). Geology of Menderes Massif and Lycian Nappes to the south of Denizli. Bulletin of the Mineral Research and Exploration 109: 37–51.

Önhon E, Ertan I, Güler S, Nazik M, Kaplan A (1989). Research on the Origin of the Karst Waters in Yukarı Çürüksu Plain Using Isotope Techniques. Final Report. State Hydraulic Works, Ankara,Turkey.

Özkaymak Ç (2015). Tectonic analysis of the Honaz Fault (western Anatolia) using geomorphic indices and the regional implications. Geodinamica Acta 27: 109–128. doi: 10.1080/09853111.2014.957504

Özkul M, Kele S, Gökgöz A, Shen CC, Jones B et al. (2013). Comparison of the Quaternary travertine sites in the Denizli Extensional Basin based on their depositional and geochemical data. Sedimentary Geology 294: 179–204. doi: 10.1016/j.sedgeo.2013.05.018

Özkul M, Varol B, Alçiçek MC (2002). Depositional environments and petrography of the Denizli travertines. Bulletin of the Mineral Research and Exploration 125: 13–29.

Özler HM (2000). Hydrogeology and geochemistry in the Çürüksu (Denizli) hydrothermal field, western Turkey. Environmental Geology 39 (10): 1169–1180. doi: 10.1007/s002540000139

Özler HM (1999). Water balance and water quality in the Çürüksu Basin in WesternTurkey. Hydrogeology Journal 7: 405–418. doi: 10.1007/s100400050212

Panichi C, Tongiorgi E (1976). Carbon isotopic composition of CO_2 from springs, fumaroles, mofettes and travertines of central and southern Italy: a preliminary prospection method of geothermal areas. In: 2nd UN Symposium on the Development and Use of Geothermal Resources. San Francisco, USA. pp. 815–825.

Parkhurst DL, Appelo CAJ (1999). User's guide to PHREEQC (version 2) – a computer program for speciation, batch-reaction, one-dimensional transport, and inverse geochemical calculations. US Geological Survey Water-Resources Investigations Report 99–4259.

Pastorelli S, Marini L, Hunziker JC (1999). Water chemistry and isotope composition of the Acquarossa thermal system, Ticino, Switzerland. Geothermics 28: 75–93. doi: 10.1016/S0375-6505(98)00045-5

Pentecost A (editor) (2005). Travertine: New York, USA: Springer-Verlag.

Rimstidt JD, Barnes HL (1980). The kinetics of silica-water reaction. Geochimica et Cosmochimica Acta 44 (11): 1683-1699. doi: 10.1016/0016-7037(80)90220-3

Rizzo AL, Uysal IT, Mutlu H, Ünal İmer E, Dirik K et al. (2019). Geochemistry of fluid inclusions in travertines from western and northern Turkey: inferences on the role of active faults in fluids circulation. Geochemistry, Geophysics, Geosystems 20 (11): 5473–5498. doi: 10.1029/2019GC008453

Roche V, Bouchot V, Beccaletto L, Jolivet L, Guillou-Frottier L et al. (2019). Structural, lithological, and geodynamic controls on geothermal activity in the Menderes geothermal Province (Western Anatolia, Turkey). International Journal of Earth Sciences 108 (1): 301–328. doi: 10.1007/s00531-018-1655-1

Schoeller H (1934). Les echanges de bases dans les eaux souterraines; trois exemples es Tunisie. Bulletin de la Société géologique de France 4: 389–420.

Semerci Aygün B (2019). Pınarbaşı Karst Kaynağının (Honaz-Denizli) Boşalım Hidrodinamiği ve Hidrokimyasal Özelliklerinin İncelenmesi. MSc, Pamukkale Üniversity, Denizli, Türkiye (in Turkish).

Şimşek Ş (1985). Geothermal model of Denizli-Sarayköy-Buldan area. Geothermics 14: 393–417. doi: 10.1016/0375-6505(85)90078-1

Şimşek Ş (2003). Hydrogeological and isotopic survey of geothermal fields in the Büyük Menderes graben, Turkey. Geothermics 32: 669–678. doi: 10.1016/S0375-6505(03)00072-5

Şimşek Ş (2005). Research on isotope techniques for exploitation of geothermal reservoirs in Western Turkey, In: Use of isotope techniques to trace the origin of acidic fluids in geothermal systems. Vienna, Austria: IAEA TECDOC Publication. pp. 155–169.

Tarcan G (2005). Mineral saturation and scaling tendencies of waters discharged from wells (>150 °C) in geothermal areas of Turkey. Journal of Volcanology and Geothermal Research 142: 263–283. doi: 10.1016/j.jvolgeores.2004.11.007

Truesdell AH (1976). Geochemical techniques in exploration. Summary of section III. In: Proceedings of the Second United Nations Symposium on the Development and Use of Geothermal Resources. San Francisco, California, USA. pp. iii-xxix.

TS266 (2005). Waters intended for human consumption (İnsani tüketim amaçlı sular), ICS 13.060.20, Turkish Standards Institution, Ankara. (in Turkish)

Uysal T, Feng Y, Zhao J, Altunel E, Weatherley D et al. (2007). U-series dating and geochemical tracing of late Quaternary travertines in co-seismic fissures. Earth and Planetary Science Letters 257 (3-4): 450–462. doi: 10.1016/j.epsl.2007.03.004

Wang X, Lu G, Hu BX (2018). Hydrogeochemical characteristics and geothermometry applications of thermal waters in coastal Xinzhou and Shenzao Geothermal Fields, Guangdong, China. Geofluids, Article ID 8715080: 1–24. doi: 10.1155/2018/8715080

Zeebe RE (2010). A new value for the stable oxygen isotope fractionation between dissolved sulfate ion and water. Geochimica et Cosmochimica Acta 74 (3): 818–828. doi: 10.1016/j.gca.2009.10.034